IMPACT OF MICROPLASTICS ON THREE LIFE-HISTORY STAGES OF STONY CORALS

YUEN CHUE HO

MPhil

The Hong Kong Polytechnic University

2025

The Hong Kong Polytechnic University

Department of Food Science and Nutrition

Impact Of Microplastics On Three Life-history Stages of Stony Corals

Yuen Chue Ho

A thesis submitted in partial fulfilment of the requirements for the degree of Master of Philosophy

April 2025

CERTIFICATE OF ORIGINALITY

I hereby declare that this thesis is my own work and that, to the best of my knowledge and belief, it reproduces no material previously published or written, nor material that has been accepted for the award of any other degree or diploma, except where due acknowledgement has been made in the text.

_____ (Signed)

Yuen Chue Ho

ABSTRACT

Microplastic (MP) pollution is a growing threat to corals, particularly those are adjacent to the dense urban and industrial area. The current study aims to bridge a knowledge gap by examining life-stage-dependent responses of stony corals to microplastics, with emphasis on the early ontogenetic windows. Specifically, this work quantified the settlement, growth and photophysiological performance of *Acropora tumida* under controlled exposures that unravelled the roles of substrate conditioning and polymer identity.

Coral planulae were reared in the laboratory and assigned to four treatments: Control, *Symbiodinium* (Zx; 900 000 cells L^{-1}), polystyrene (PS; 900 000 particles L^{-1}) and a Mix (900 000 cells L^{-1} & 900 000 particles L^{-1}). Treatments were applied in parallel on biofilm-conditioned versus unconditioned ceramic tiles. In a second experiment, twelve-month-old juveniles and field-collected adult fragments were exposed for 30 days to polypropylene (PP; 10 mg L^{-1}), polyethylene terephthalate (PET; 10 mg L^{-1}) or natural sediment (10 mg L^{-1}); growth (surface area, polyp budding, buoyant weight) and photochemistry (Fo, Abs, Fv/Fm) were tracked with imaging-PAM fluorometry. Field surveys at four sites compared microplastics in *Platygyra acuta* skeletons with adjacent sediments in Mirs Bay.

The experimental findings were stage specific. Unconditioned tiles reduced larval settlement by 74–95 % although post-settlement growth increased slightly (≈ 3–8 %). On conditioned tiles, the Mix treatment suppressed settlement by 38 %, indicating that PS-altered symbiont cues can nullify positive biofilm signals. In juveniles, PP significantly reduced tissue growth, polyp number and photochemical efficiency, whereas PET and sediment produced negligible effects. Adults remained mostly unaffected, with similar buoyant weight and Fv/Fm values to controls.

Field results showed that coral skeletons incorporated microplastic concentrations up to ten times higher than nearby sediments. The particles sizes were dominated by polyethylene fragments (30–100 μm) and reflecting stronger input from urban sources. Collectively, the findings indicated that microplastic effects depend on both coral life stage and polymer type. Comparing to Adults, juveniles are the more sensitive. These results highlight the need for

reducing polymer-specific inputs and for conservation measures that prioritise the protection of early coral life stages in coastal waters with high microplastic loads.

ACKNOWLEDGEMENTS

I would first like to thank my supervisor prof James Kar-Hei Fang for inviting me to join his research group. His clear guidance and steady encouragement helped me test ideas, make mistakes, and learn from them. His door was always open, and that made a big difference.

I am also grateful to prof Apple Pui-Yi Chui at CUHK. She arranged lab space, equipment, and permits when I needed them most. Her practical advice and calm support kept this project moving forward.

My thanks go to my lab mates at PolyU. Your help with experiments, long discussions over coffee, and good humour turned long hours in the lab into enjoyable days. I also thank my friends at CUHK for early-morning dives and many shared laughs. These moments kept my spirits up.

Finally, I owe my deepest thanks to my family, partner, and close friends. Your patience, understanding, and constant belief in me gave me the strength to face every challenge. This thesis would not exist without your love and support.

TABLE OF CONTENTS

ABSTRACT ..... *III*

ACKNOWLEDGEMENTS ..... *V*

TABLE OF CONTENTS ..... *VI*

List of figures ..... *IX*

List of tables ..... *XIV*

Chapter 1 – Introduction *1*

1.1 Background **1**

1.2 Microplastic pollution on coral larvae **2**

1.3 Microplastic pollution on juvenile and adult corals **3**

1.4 Microplastics in local corals and habitats **5**

1.5 Aims and Objectives **7**

Chapter 2 – Materials and method *8*

2.1 Experiment 1 – Effect of microplastics and zooxanthellae on larvae under different substrate conditions **8**

2.1.1 Samples collection 8

2.1.2 Treatments preparation 10

2.1.3 Measurements on larval settlement & growth 11

2.1.4 Measurements on microplastic ingestion 12

2.2 Experiment 2 – Effect of microplastics and sediments on juvenile and adult corals **12**

2.2.1 Samples collection 12

2.2.2 Treatments preparation 13

2.2.3 Measurements on growth, photosynthesis and bleaching 13

2.3 Microplastics in corals and habitats in Mirs Bay **15**

2.3.1 Samples collection 15

2.3.2 Microplastics extraction procedure 16

2.3.3 Microplastics identification 18

2.3.4 Three dimensions scanning of coral fragments 19

2.4 Statistical Analyses **20**

2.4.1 Statistical Framework and Model Specification 20

2.4.2 Experiment-Specific Model Structures....21

Chapter 3 – Result ***23***

3.1 Larval settlement and growth **23**

3.1.1 Overview of settlement rate and growth rate....23

3.1.2 Bayesian Posterior Modelling....24

3.1.3 Bayesian Hypothesis Testing....24

3.1.4 Variance Decomposition....26

3.1.5 MPs ingestion....27

3.2 Growth and photosynthesis of juvenile and adult corals **28**

3.2.1 Effects of MPs and sediment on the growth capability of juvenile *A. tumida*....28

3.2.2 Effects of MPs and sediment on the photochemical performance of zooxanthellae in juvenile *A. tumida*....31

3.2.3 Effects of MPs and sediment on the growth capability of adult *A. tumida*....36

3.2.4 Effects of MPs and sediment on the photochemical performance of zooxanthellae in adult *A. tumida*....38

3.3 Distribution of microplastic in habitats and coral compartments **43**

3.3.1 Spatial comparison of MPs in corals and habitat sediments....43

3.3.2 Characteristics of MPs....44

3.3.3 Comparison of total MPs concentrations in coral skeletons and habitat sediments....46

3.3.4 Comparison of polymer type composition (PE, PET, PS, PP) in coral skeletons and habitat sediments....47

3.3.5 Microplastics distribution in corals....50

Chapter 4 – Discussion ***52***

4.1 Impacts of Microplastics on coral larvae **52**

4.1.1 Influence of substrate conditioning and microplastics on larval settlement....52

4.1.2 Limited impact of microplastics on larval growth and ingestion of microplastics....53

4.2 Impacts of microplastics on juvenile and adult coral **55**

4.2.1 Life-stage dependent Sensitivity to microplastics....55

4.2.2 Different toxicity of microplastic polymers....56

4.3 Distribution of microplastics in corals and habitats in Mirs Bay **58**

4.3.1 Coral skeletons as a long-term Sink....58

4.3.2 Spatial and sample-type patterns in polymer composition....59

Chapter 5 - Conclusion ***61***

Limitations and further studies **62**

Reference ***63***

List of Figures

Figure 2. 1 (a) Hard coral community in the Tung Ping Chau Marine Park, showing a high biodiversity in the northeastern waters of Hong Kong; (b) the branching coral *Acropora tumida*. 9

Figure 2. 2 (a) Gametes of *Acropora tumida* collected from the Tung Ping Chau Marine Park for the experiments 9

Figure 2. 3 Coral culture in laboratory: **(a)** eggs and sperm of *Acropora tumida* mixed and fertilised; **(b)** a planula larva recently settled on a tile; **(c)** a coral polyp one month and **(d)** two months after settlement, and **(e)** its development into a juvenile with multiple polyps for 12–14 months. 9

Figure 2. 4 Images of the tile, inclusive of a scale for reference, were captured using a digital camera (canon 200d: resolution 24.2 megapixels) in combination with a macro lens (Laowa 90mm f/2.8 2x Ultra Macro APO) and a speed flash (Godox TT685II). The settled coral larvae are denoted by a white arrow in the image. 11

Figure 2. 5 (a) Part of the hatchery facilities used in this project to produce coral larvae of *A. tumida* for **(b)** the experimental setup; **(c)** stereomicrograph showing planula larvae (black arrowed), a settling larva (grey arrowed) and a settled larva (white arrowed). 12

Figure 2. 6 Preparation of microplastics. (a) Plastic egg carton represents a common domestic waste of polyethylene terephthalate (PET) and (b) were cryogenically ground at –196 °C using a Retsch CryoMill (Haan, Germany) to produce (c) plastic particles of PET for the experiments. Likewise, microplastics of polypropylene (PP) were prepared from the same batch of disposable PP cups using the CryoMill.....14

Figure 2. 7 Coral fragments of *A. tumida* and assessed with a Maxi Imaging-PAM chlorophyll fluorometer (Walz, Germany). Photosynthesis-related parameters were measured, including maximum and minimum fluorescence yields (Fm and Fo, respectively, indicating the maximum light harvesting capacity and relative amount of chlorophyll a), and maximum quantum yield of photosystem II (Fv/Fm, representing the efficiency to process captured photons for photosynthesis). Absorptivity (Abs), another indicator of the relative amount of chlorophyll a, was also measured. Relative values are displayed using an identical colour scale, which ranges from 0 (black) to 1 (purple) as shown at the bottom. Juvenile *A. tumida* was assessed using the same method. 14

Figure 2. 8 QGIS map of Mirs Bay indicating the sampling sites of *Platygyra acuta*. Areas shaded in grey and dark grey represent Hong Kong and Shenzhen, respectively, while blue denotes hydrology. The locations of the four sampling sites are marked with crosses. 15
Figure 2. 9 The workflow for analyzing microplastics in the laboratory using a Renishaw inVia confocal Raman microscope (Wotton-under-Edge, UK; see Ho et al. 2022); (b) Examples of microplastics identified from the coral and sediment samples in Part III and their Raman spectra compared to the reference spectra.....19
Figure 2. 10 (a) The University Research Facility in 3D Printing (U3DP) at The Hong Kong Polytechnic University, where (b) fragments of *P. acuta* were scanned using an EinScan Pro 2X handheld 3D scanner (Shining 3D, China) to determine the tissue surface area. 19

Figure 3. 1 Settlement and growth of *A. tumida* larvae after 60 days. white dots = mean; lines = median; boxes = interquartile range (IQR); whiskers = data spread; dashed vertical line = 100 %, the reference value.....23
Figure 3. 2 Bayesian GLMM Posterior estimates and credible intervals for standardized settlement (A) and growth (B). Dots = medians; Lines = 50%, 89% and 95% CI. Dashed line separates tile conditions. Posterior R^2 values indicates model explanatory power.....24
Figure 3. 3 Posterior estimates for standardised settlement (A) and growth (B) across treatments and tile conditions. Density plots show effect size between treatment pairs: i) within conditioned tiles, ii) within unconditioned tiles, iii) across tile conditions; lines (50 %, 89 % & 95 % CI); colour (red = positive, blue = negative, grey = non-significant). Estimates are based on standardised model outputs.....26
Figure 3. 4 Variance decomposition for larval responses: Settlement rate (A) and growth rate (B). Percentage scales show contributions from treatment, tile condition, and interactions. Dots = medians variance proportions; bars = IQR; lines = 95% CI. Percentage scales show contributions from treatment, tile condition, and interactions. 27
Figure 3. 5 Zooxanthellae (Zx; *Symbiodinium clade C1*) inoculation in larvae under different conditions. Fluorescent micrographs show normal symbiont uptake without MPs (A) and simultaneous incorporation of PS particles (10 μm) during symbiont acquisition (B). Images were captured using a Nikon Eclipse Ti2-E live-cell imaging system, demonstrating PS internalization by the coral host. 27
Figure 3. 6 Morphological responses of juvenile corals to MPs exposure. Surface area (A) and polyp count (B) are shown across treatments (Control, PP, PET, Sediment). White dots = means; lines = median; Boxes = IQR; whiskers = data spread. 29

Figure 3. 7 Bayesian GLMM posterior distributions of MPs and sediment exposure on juvenile coral growth. Standardised surface area (a) and polyp count (b) are presented for treatments (Control, PP, PET, Sediment). Black dots = medians; lines = 50%, 89% & 95% CI; R^2 indicates model explanatory power. 29
Figure 3. 8 Posterior estimates and hypothesis testing of juvenile coral growth under MP and sediment exposure. Standardised surface area (A) and polyp count (B) are shown across treatments (Control, PP, PET, Sediment). Density plots display effect sizes; lines = 50%, 89% and 95% CI; colours (blue = negative, red = positive, grey = non-significant) indicate statistical support. Estimates are based on standardised model outputs. 31
Figure 3. 9 Photochemical responses of zooxanthellae in juvenile corals following exposure to MPs and sediment. Grey scale (A), Abs (B), Fo (C), and Fv/Fm (D) are shown across treatments (Control, PP, PET, Sediment). Dots = means; Lines = medians; Boxes= IQR; whiskers = data spread. 33
Figure 3. 10 Bayesian GLMM posterior distributions and CI of photochemical performance of juvenile corals exposed to MPs and sediment. Standardised grey scale (A), Abs (B), Fo (C), and Fv/Fm (D) are shown across treatments (Control, PP, PET, Sediment). Dots = medians, and lines = 50%, 89%, and 95% CI. Posterior R^2 values indicate model explanatory power. 34
Figure 3. 11 Posterior estimates of photochemical responses in juvenile corals exposed to MPs and sediment. Standardised grey scale (A), Abs (B), Fo (C), and Fv/Fm (D) are shown across treatments (Control, PP, PET, Sediment). Density plots represent the effect size between treatments; line = 50%, 89%& 95% CI and colours (blue=negative, red=positive, grey=non-significant) indicate statistical support. Estimates are based on standardised model outputs. 35
Figure 3. 12 Observed and modelled buoyant weight of adult corals following exposure to MPs and sediment. (A) Boxplots show observed buoyant weights. Dots = means; lines = medians; Boxes = IQR; whiskers = data spread. (B) Bayesian GLMM posterior distributions and CI of standardized buoyant weight. Dots = medians, and lines = 50%, 89% & 95% CI. Posterior R^2 values indicate model explanatory power. 36
Figure 3. 13 Posterior estimates and hypothesis testing of adult corals growth under MPs and sediment exposure. Density plots represent the effect size between treatments. Lines = 50%, 89% & 95% CI. colours (blue=negative, red=positive, grey=non-significant) indicate statistical support. Estimates are based on standardised model outputs. 37
Figure 3. 14 Photochemical responses of zooxanthellae in adult corals following exposure to MPs and sediment. Grey scale (A), Abs (B), Fo (C), and Fv/Fm (D) are shown across treatments

(Control, PP, PET, Sediment). Dots = means; Boxes = IQR; lines = medians; whiskers = data spread. 39
Figure 3. 15 Bayesian GLMM posterior distributions and CI of photochemical responses in zooxanthellae in adult corals following exposure to MPs and sediment. Standardised grey scale (A), Abs (B), Fo (C), and Fv/Fm (D) are shown across treatments (Control, PP, PET, Sediment). Dots = medians, and lines = 50%, 89% & 95% CI. Posterior R^2 values indicate model explanatory power. 40
Figure 3. 16 Posterior estimates and hypothesis testing of photochemical responses in zooxanthellae in adult corals under MPs and sediment exposure. Standardised grey scale (A), Abs (B), Fo (C), and Fv/Fm (D) are shown across treatments (Control, PP, PET, Sediment). Density plots represent the effect size between treatments. Lines = 50%, 89% & 95% CIs and colours (blue=negative, red=positive, grey=non-significant) indicate statistical support. Estimates are based on standardised model outputs. 42
Figure 3. 17 QGIS maps of Mirs Bay showing the spatial distribution of MP concentrations in (A) sediments, (B) coral tissue, and (C) skeletons across four *P. acuta* habitats. Warmer colours (orange) indicate higher concentrations, while cooler colours (blue) represent lower concentrations. 43
Figure 3. 18 Distribution and characteristics of MPs (MPs) across sampling sites. (A) Percentage of MPs by size class; (B) Percentage of polymer types; (C) Percentage of colours; (D) Percentage of particle shapes. 45
Figure 3. 19 Observed and modelled total MPs concentrations across sites and tissue types. (A) Boxplots show observed MPs concentrations (items cm^{-3}). Dots = means, lines = medians, boxes = IQR, whiskers = data spread. (B) Bayesian GLMM posterior distributions and CI of standardized total MPs concentrations. Dots = medians, and lines = 50%, 89% & 95% CI. Posterior R^2 values indicate model explanatory power. 46
Figure 3. 20 Posterior estimates and hypothesis testing of standardised MPs concentrations across sites and tissue types. Density plots represent the effect size between pairs: i) sites within coral skeletons, ii) sites within sediments, iii) skeletons vs sediments within same site. Lines = 50%, 89% & 95%CI. Colours (blue=negative, red=positive, grey=non-significant) indicate statistical support. Estimates are based on standardised model outputs. 47
Figure 3. 21 Polymer-specific MPs concentrations in coral skeletons and habitat sediments. Boxplots show concentrations of PE (A), PET (B), PP (C), and PS (D) across sites (CI, DI, PI, and TPC). Dots = means, boxes = IQR, lines = medians, whiskers = data spread. Coral skeletons are shown in the upper shaded panels and sediments in the lower panels. 48

Figure 3. 22 Bayesian GLMM posterior distributions and CI of polymer-specific MPs concentrations in coral skeletons and habitat sediments. Standardised logit-scale concentrations of PE (A), PET (B), PP (C), and PS (D) are shown across sites (CI, DI, PI, and TPC). Dots = medians, and lines = 50%, 89% % 95% CI. Posterior R^2 values indicate model explanatory power. Coral skeletons are shown in the upper shaded panels and sediments in the lower panels. 49

Figure 3. 23 Posterior estimates and hypothesis testing of polymer-specific MPs concentrations in coral skeletons and habitat sediments. Standardised logit-scale concentrations of PE (A), PET (B), PP (C), and PS (D) are shown across sites (CI, DI, PI, and TPC). Density plots represent the effect size between pairs: i) sites within coral skeletons, ii) sites within sediments, iii) skeletons vs sediments within same site. Lines = 50%, 89% & 95% CI; colours (blue = negative, red = positive, grey = non-significant) indicate statistical support. Estimates are based on standardised model outputs. 50

Figure 3. 24 Comparison of MPs distribution in coral tissues and skeletons, standardised by tissue area (160.4 cm^2) and skeleton volume (115.8 cm^3), respectively. 51

List of Tables

Table 3. 1 Summary of Bayesian model estimates for juvenile *A. tumida* growth capability relative to control group. The table shows the 89% and 95% CI, percentage of the posterior distribution within the Region of Practical Equivalence (ROPE; ±0.1), and the probability of direction (PD). Lower ROPE and higher PD values suggest more meaningful treatment effects. 30

Table 3. 2 Summary of Bayesian model estimates for the photochemical performance of zooxanthellae in juvenile *A. tumida* relative to control group. The table shows the 89% and 95% CI, percentage of the posterior distribution within the Region of Practical Equivalence (ROPE; ±0.1), and the probability of direction (PD). Lower ROPE and higher PD values suggest more meaningful treatment effects. 35

Table 3. 3 Summary of Bayesian model estimates for adult *A. tumida* growth capability (buoyant weight) relative to control group. The table shows the 89% and 95% CI, percentage of the posterior distribution within the Region of Practical Equivalence (ROPE; ±0.1), and the probability of direction (PD). Lower ROPE and higher PD values suggest more meaningful treatment effects. 37

Table 3. 4 Summary of Bayesian model estimates for the photochemical performance of zooxanthellae in adult *A. tumida* relative to control group. The table shows the 89% and 95% CI, percentage of the posterior distribution within the Region of Practical Equivalence (ROPE; ±0.1), and the probability of direction (PD). Lower ROPE and higher PD values suggest more meaningful treatment effects. 41

Chapter 1 – Introduction

1.1 Background

Plastics have become indispensable in modern daily life, with global annual production exceeding 360 million tones and continuing to rise ("Plastics Europe," 2021). These synthetic polymers are as a byproduct of petroleum and characterized by their chemical diversity, inertness, and durability. As invented in the 19th century, plastics gain popularity due to their versatility and cost-effectiveness. Due to the excellent durability and plasticity, plastic usage surge and was once considered as an environmentally friendly alternative to wood. Fo example, the inventor of the plastic bag intended to replace paper bags.

However, public perception has shifted as severe environmental issues are caused by increasing plastic consumption and inadequate waste management. One of the concerns is marine plastic pollution. By estimation, over five trillion pieces of plastic debris are floating in the sea and thus number may be doubled by 2025 (Eriksen et al., 2014; Jambeck et al., 2015). Plastic debris within the size range of 1–5000 μm is classified as microplastics. These small particles enter the marine environment through direct sewage discharge (Bashir et al., 2021; Liu et al., 2021; Mak et al., 2020) and indirectly the fragmentation of larger plastic items, broken down by photochemical oxidation, wave action and other degradation mechanisms (Zhang et al., 2021).

Microplastics have become ubiquitous globally. They are detected in remote environments, including the Tibetan Plateau at 4000 meters above sea level (Liang et al., 2022), the Canadian Arctic Ocean at depths of 1000 meters (Ross et al., 2021), and even within the human body (Ho et al., 2022). Environmental records show a dramatic increase in microplastic concentrations worldwide, up to a two-order-of-magnitude increase in the Pacific Ocean (Brandon et al., 2019; Goldstein et al., 2012; Lavers & Bond, 2017). The extent of this contamination suggests that marine organisms are experiencing a wide range of exposure scenarios.

Given the global scale and pervasive nature of microplastic pollution, understanding its ecological implications are crucial, especially for marine ecosystems where threaten by

microplastics but not yet fully understood. Coral habitats, recognized as one of the most diverse and valuable marine ecosystems, are threaten by increasing stresses from microplastics. However, detailed studies on impacts of local coral remain mostly unknown, creating a knowledge gap. It is essential to explore how microplastics interact with corals and their symbiotic relationships, which determines the health and productivity of coral communities.

Among marine organisms, scleractinian corals are particularly vulnerable to microplastics (MPs) due to their suspension-feeding mechanisms and dependence on symbiotic relationships. These benthic organisms help maintaining reef ecosystem stability. Any disruption to their health can significantly affect overall reef productivity and resilience (Pantos, 2022). Recent research indicates that ingestion of MPs by corals can reduce feeding efficiency, trigger inflammation, induce oxidative stress, and interfere some crucial physiological processes (Tang et al., 2024). In addition, MPs may disrupt the symbiotic relationship between corals and zooxanthellae (*Symbiodinium* spp.), which support growth and survival of corals (Okubo et al., 2018). To better understand these impacts, in-depth studies is necessary.

1.2 Microplastic Pollution on Coral Larvae

Microplastics (MPs), originating from terrestrial sources, threatens coastal coral habitats more compared to offshore ecosystems (Huang et al., 2021). Hard corals, also known as *Scleractinia*, are particularly susceptible due to their inability to differentiate MPs from natural food particles (Hall et al., 2015). Ingestion rates of MPs by corals have been reported to be ten times higher than those of sand particles, potentially due to the presence of phagostimulants in microplastics that promote ingestion (Allen et al., 2017). While some MPs are expelled, others may persist within the coral gastrovascular cavity, resulting in oxidative stress, physical obstruction, and reduced feeding efficiency (Pantos, 2022; Soares et al., 2020).

Corals of early life stages are particularly susceptible to stress owing to their immature development and smaller biomass (Jiang et al., 2017; Liu et al., 2020). Corals utilize both passive (mucus secretion) and active (ciliary currents and tentacles) mechanisms for feeding (Sebens et al., 1998). However, presence of phagostimulants on microplastics can cause inability to distinguish MPs from edible particles and thus ingestion (Allen et al., 2017). The

resulted adverse impacts include gastrovascular blockage, reduced feeding, elevated metabolic demands for egestion, bleaching and necrosis (Lanctot et al., 2020; Pantos, 2022; Savinelli et al., 2020; Soares et al., 2020; Syakti et al., 2019). Accordingly, this study quantifies MP ingestion rates in larval *Acropora tumida,* which is fast growing and important to reef accretion (Mercado-Molina et al., 2020).

Another essential early life stage process is larval settlement, which relies heavily on chemical cues emitted by reef substrates. Previous studies have demonstrated that sediment deposition can suppress settlement or smother newly settled larvae (Babcock & Davies, 1991; Babcock & Mundy, 1996). The effect is exacerbated by benthic algae which reduced water flow and promoted the accumulation of sediments (Howlett, 1995). Similar mechanisms may apply to suspended microplastics, which may obstruct larval-substrate interactions and delay or prevent successful settlement. Therefore, the current study assessed larval settlement on two types of substrates: conditioned (with natural biofilm colonization) and unconditioned (biofilm-free).
The acquisition of zooxanthellae is critical during early development, as these symbionts can support energy requirements by supplying carbohydrates and proteins and aiding in waste removal. Studies show about 70% of photosynthesis fixed carbon is translocated from symbiont to host (Gaither & Rowan, 2010), and up to 95% energy requirement of host can be met by symbiosis (Falkowski et al., 1993). Rapid post-settlement growth is vital for larvae to outcompete other competitors. Aposymbiotic larvae, lacking zooxanthellae, exhibit slower growth and reduced survival potential (Harii et al., 2010). Microplastics may not only induce oxidative stress in corals but also disrupt the symbiosis process (Chen et al., 2022; Okubo et al., 2018). Successful larval settlement and symbiont acquisition are therefore essential for early coral development and resilience. To evaluate this, experiment should be carried out to study the impacts of microplastics on larval settlement and growth.

1.3 Microplastic Pollution on Juvenile and Adult Corals

Understanding the potential impacts of microplastics on coral recruits and adults is essential, given their important roles in coral ecosystems. Coral recruits represent the transitional stage from larvae to adult. Their successful development determines long-term resilience of coral communities. Adult corals, on the other hand, provide the seabed structure and ecological function through growth and reproduction. Investigating the impacts of microplastics on two

life stages provides valuable insights into coral sustainability under increasing microplastic pollution.

Previous studies indicate microplastics can influence coral growth through energy allocation disruption and physical interference. Adult corals mistakenly ingest MPs due to presence of phagostimulant on the surface of microplastics, particularly biofouled particles (Allen et al., 2017). Energy expended in mucus production and ciliary action to remove ingested plastics directly compromises energy availability for calcification and growth processes (Reichert et al., 2019; Rotjan et al., 2019). The potential impacts on the growth of coral recruits could be more severe. Juveniles, with minimal tissue reserves and fragile structures, may be more vulnerable. Growth suppression may occur due to continuous mucus shedding and reduced feeding efficiency induced by microplastics adherence and ingestion (Axworthy & Padilla-Gamino, 2019; Berry et al., 2019). The recruit survivability can directly influence population recovery so understanding growth impacts at this sensitive life stage is urgent. However, the extent of these mechanisms affects coral recruits, compared to adults, remains understudied and requires investigation.

Coloration changes, related to compromised symbiotic relationships, are indicators of stress induced by microplastics. The colour of corals relies on the density and health of zooxanthellae. Microplastics exposure may induce stress through shading and physical irritation, causing zooxanthellae loss and bleaching. Studies document rapid and significant bleaching in *Acropora formosa* following short-term exposure to microplastics, particularly smaller particles that easily adhere to coral tissues (Syakti et al., 2019). Juvenile corals, given their smaller size and limited symbiont reservoirs, may experience higher susceptibility to such stress-induced bleaching events. Given the dependence of recruits on symbiotic relationships for energy acquisition, bleaching can directly limit their growth potential and survival rates (Berry et al., 2019). Apart from loss of zooxanthellae, photosynthetic efficiency is also crucial for coral survival and growth. Microplastics deposited on coral surfaces reduce available light for photosynthesis while particle ingestion and internal stress mechanisms further degrade photosynthetic performance. Some studies suggest photochemical efficiency is reduced in coral symbionts exposed to microplastics (Lanctot et al., 2020; Reichert et al., 2019). However, whether coral recruits respond differently from adults remains inadequately explored. For coral recruits, impaired photosynthesis could critically limit energy availability, given their limited capacity for heterotrophic feeding at this stage. However, comparing these impacts across coral

life stages is still relatively scarce, highlighting a possible knowledge gap. Therefore, the current study aims to investigate and compare microplastics impacts on coral recruits and adults, focusing on key physiological metrics: growth, coloration changes, and photosynthetic efficiency.

1.4 Microplastics in Local Corals and Habitats

Hong Kong is a densely populated and industrialized coastal city and locates at the mouth of the Pearl River Delta. It faces substantial marine debris challenges. Previous studies have documented widespread microplastic (MP) pollution in local waters and beaches (Lo et al., 2018; Tsang et al., 2017), with Tolo Harbor ranking among the most contaminated sites worldwide (Leung et al., 2021). Although these studies have addressed MP pollution in urban coastal environments, little is known about the occurrence of MP within coral habitats.

Mirs Bay, on the eastern coast of Hong Kong, is one of the most important local coral habitats. The Bay is relatively distant from the major pollution hotspot, Pearl River Delta. Contamination in the Bay is primarily influenced by local sources (Morton, 1994). Potential sources of microplastics in Mirs Bay include local terrestrial runoff and shipping activity, particularly near the Yantian International Container Terminal (Bashir et al., 2021; Cho et al., 2023). Importantly, these pressures are adjacent to Yan Chau Tong and Tung Ping Chau Marine Parks, which served as the study sites. These parks represent ecologically valuable and legally protected areas, and thus priority locations for assessing MP contamination. Investigating MPs in such refuges provides critical insights into pollution risks within habitats designated for coral conservation.

Despite their ecological importance, few studies in Hong Kong have examine MP contamination in both corals and their surrounding environment. The most related study surveyed sediment microplastics in local coral habitats (Cheang et al., 2018). No study has examined MPs within coral in this area. Understanding how microplastics distribute across coral body compartments helps to evaluate the partition of MPs in soft tissues and skeleton. These body parts may incorporate MPs through different pathways and results different mode of accumulation. Particles once locked in skeleton may serve as a long-term sink (Reichert et al., 2022). However, the extent of microplastic incorporated compared to nearby environment

remains mostly unknown. To address this gap, the present study investigates the abundance and polymer composition of microplastics in paired samples of corals and adjacent sediments.

A key barrier to progress is methodological. MPs embedded in coral skeletons or entangled in soft tissues are difficult to extract without damaging polymers. Conventional protocols rely on density separation or chemical digestion to remove organic and mineral fractions. While NaCl based flotation is inexpensive, it recovers only low-density polymers. Denser solutions such as $ZnCl_2$ or NaI provide broader polymer recovery but may be less accessible (Leung et al., 2021; Lo et al., 2018; Rani et al., 2023; Tsang et al., 2017). Similarly, digestion methods differ in effectiveness: alkaline and oxidative treatments efficiently clear organic matter, whereas acid-based methods are needed for calcareous skeletons but risk degrading sensitive polymers (Cole et al., 2014; Malik et al., 2022). Comparing and adapting these techniques is therefore essential for accurate MP recovery from different coral compartments.

Polymer identification also presents challenges. Earlier coral research often relied on Fourier Transform Infrared (FTIR) spectroscopy or visual identification. However, these methods are time-consuming and complex in sample preparation, involving manual picking and inspection of small particles (Brandt et al., 2020; Huang et al., 2023). In contrast, Raman spectroscopy with automated mapping has emerged as a powerful alternative. This technique allows direct particle scanning on filters, improved resolution for small fragments, and reduced handling error.

Finally, standardizing MP abundance to coral size is critical for ecological comparisons. Traditional approaches such as water displacement for volume or wax dipping for surface area suffer from low precision and practical limitations with irregular coral shapes (Herler & Dirnwober, 2011; Veal et al., 2010). For example, wax dipping, used for surface area estimation, can vary in accuracy (14%–26%). Other methods, such as 2D camera imaging for surface area estimation may fail with complex coral shapes due to the lack of depth information (Chandler et al., 2024). In contrast, 3D scanning offers high accuracy and precision (< 2%) for volume measurements (Reichert et al., 2016). It is a non-invasive, reproducible and consistent method for live coral studies.

Together, these considerations highlight the need for integrative protocols that combine reliable extraction, robust polymer identification, and accurate standardization. To address this gap, the

current study investigates the abundance and polymer composition of MPs in paired samples of corals and adjacent sediments from Mirs Bay. The current study applies methodological advances to improve detection and comparability across coral body compartments.

1.5 Aims and Objectives

The aim of this thesis is to investigate the interaction of microplastics (MPs) and scleractinia across different life stages. This research includes laboratory experiments and field study to explore the effects of microplastics on coral health and function. Specifically, the study examines the growth, ingestion and settlement of *A. tumida* larvae under the microplastic exposure. The effects on growth, coloration, and photosynthetic efficiency in juvenile and adult corals are also addressed. In addition, tailor made protocols were designed to extract and analyse MPs from soft tissues and skeletons of corals and sediments. The analysis enables a more accurate assessment of microplastics incorporation within different body compartments. This approach is applied in a field study conducted in Mirs Bay, Hong Kong, where the abundance, distribution, and polymer composition of microplastics are quantified in *P. acuta* and surrounding sediments. Collectively, these findings provide insights that are relevant for environmental monitoring, coral management, and contaminant mitigation efforts in marine ecosystems.

This thesis is structured into four chapters, each addressing different aspects of microplastic (MP) pollution and its impacts to coral communities. Chapter 1 provides an overview of global microplastic pollution and its impact on coral, including the MPs sources, distribution, and ecological implications. Chapter 2 details the experimental and analytical methods used throughout the study includes laboratory exposures on *A. tumida* larvae, recruits, and adults to various microplastic types (e.g., polystyrene, polypropylene, PET, and sediments) and field study of *P. acuta* in Mirs Bay. Chapter 3 presents the results of both laboratory and field experiments. These include microplastic ingestion, settlement patterns and growth in larvae; growth, coloration, and photosynthetic efficiency in juveniles and adults; and microplastics distribution in coral tissues, skeletons, and surrounding sediments. Chapter 4 discusses the findings regarding to coral life-stage sensitivity to microplastic exposure, potential accumulation and broader environmental implications.

Chapter 2 – Materials and Methods

2.1 Larval Responses to Microplastics and Zooxanthellae under Different Substrate Conditions

2.1.1 Samples collection

The coral larvae were collected by scuba divers and cultured in Simon F.S. Li Marine Science Laboratory for experimental use. The larvae of branching coral *Acropora tumida* (Fig. 1b) were served as the test species in this study since they are the major broadcast-spawning corals in Hong Kong and were available for collection during the study period. Its rapid growth and successful acquisition of *Symbiodinium* (zooxanthellae) during early life stages are critical for securing energy and enhancing resilience in competitive environments (Terrell et al., 2023).

Gametes of *A. tumida* were collected by scuba diving from the Tung Ping Chau Marine Park, Hong Kong (Fig. 2.1), during the spawning season in summer 2021. Collected gametes were transported to the laboratory and maintained in glass tanks with filtered natural seawater. In-vitro fertilisation and rearing of corals were performed under laboratory conditions (Chui & Ang, 2015; Chui & Ang, 2017; Chui et al., 2014). In brief, eggs and sperm were mixed for fertilisation (Fig. 2.3 a). Fertilised eggs developed into planula larvae were induced to settle on ceramic tiles (Fig. 2.3 b, 2.4 a). *Symbiodinium* (clade C1) was water-piked from local corals (Ng & Ang, 2016) and supplied to settling larvae to initiate symbiosis. The sample collection in the Tung Ping Chau Marine Park was carried out with the permission of the Agriculture, Fisheries and Conservation Department, the Government of Hong Kong SAR (permit number: 51 in AF MPD 09/3 Pt.24).

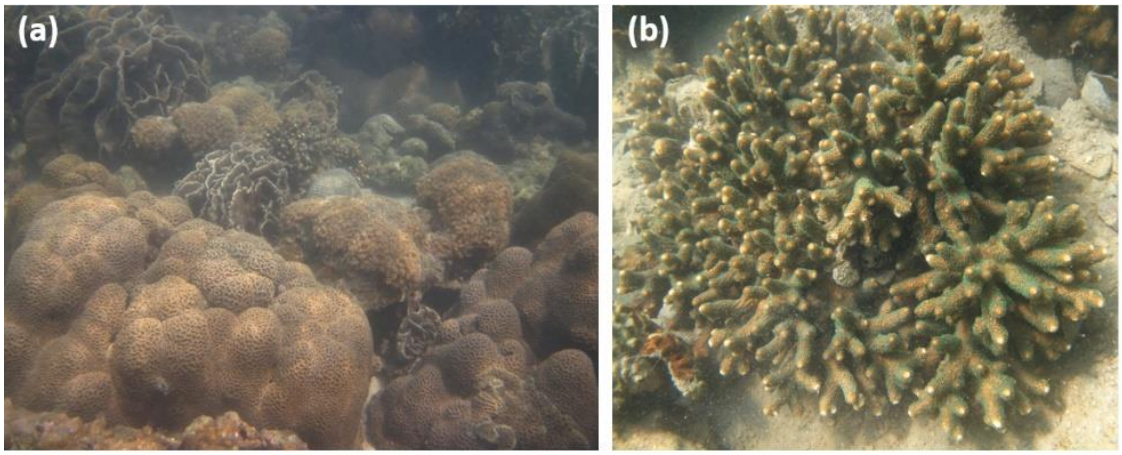

Figure 2. 1 (a) Hard coral community in the Tung Ping Chau Marine Park, showing a high biodiversity in the northeastern waters of Hong Kong; (b) the branching coral *Acropora tumida*.

Figure 2. 2 (a) Gametes of *Acropora tumida* collected from the Tung Ping Chau Marine Park for the experiments

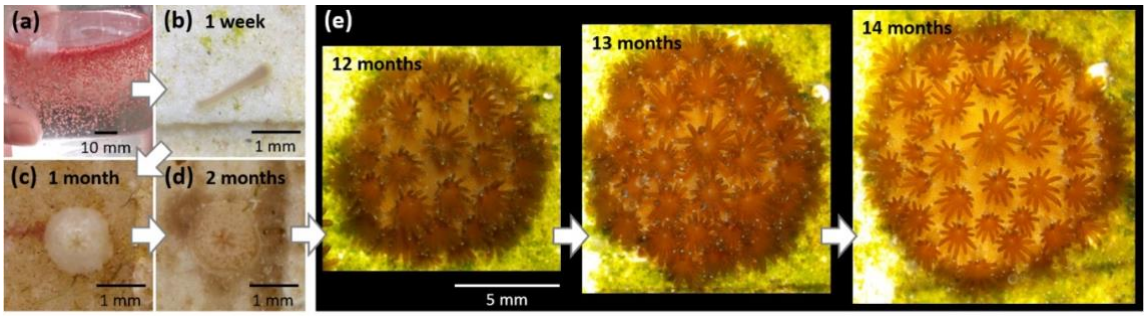

Figure 2. 3 Coral culture in laboratory: **(a)** eggs and sperm of *Acropora tumida* mixed and fertilised; **(b)** a planula larva recently settled on a tile; **(c)** a coral polyp one month and **(d)** two months after settlement, and **(e)** its development into a juvenile with multiple polyps for 12–14 months.

2.1.2 Treatments preparation

Four treatments were established: control, Zx (900,000 cells L^{-1}), PS (900,000 particles L^{-1}), and Mix (900,000 cells L^{-1} + 900,000 particles L^{-1}). The Zx treatment consisted of *Symbiodinium clade C1* extracted from *A. tumida, A. pruinosa, A. valida or P. acuta* using the water-pik method (Ng & Ang, 2016), with a random fragment selected for each dosing event.. Extracted Zx (mean diameter ≈ 10 µm) was maintained in f/2 medium using a 12:12 light-dark cycle at 150 µmol photons m^{-2} s^{-1} during the light period, until being used in the experiment. To mimic the size, shape and natural buoyancy of Zx, micro-spherical polystyrene (10µm, Fluoresbrite YG) was used as a test model (mean diameter = 10 µm; density = 1.04–1.09 g cm^{-3}). The PS particles were fluorescent (absorption at 441 nm; emission at 486 nm) to facilitate microscopic observation.

The four treatments were with three replicates each, and each replicate contained 100 coral larvae. Larvae were pipetted and counted manually using a tally counter. The control treatment contained no Zx or PS. The Zx treatment represented the natural exposure group, in which Zx and coral larvae could form symbiosis. The other two treatments assessed the larval responses to PS in the presence or absence of Zx. In all treatments, 150µl homogenised brine shrimp (*Artemia*) was added on day 0 to stimulate the feeding response of coral larvae and facilitate the Zx acquisition (Harii et al., 2009; Schwarz et al., 1999). Each replicate tank contained one litre of filtered seawater at 35 ‰ salinity, with water movement maintained by aeration of filtered air (0.45µm) (Fig. 2.5 b). The treatment media, *Artemia* and filtered seawater were renewed every 6 days carefully to avoid loss of larvae.

Artificial substrates were used to induce larval settlement. Ceramic tiles (Fang et al., 2018), were pre-conditioned for a month in Tung Ping Chau Marine Park (TPCMP) to allow colonization of natural biofilm and crustose coralline algae (Fig. 2.4), which are known to facilitate coral settlement (Petersen et al., 2004). Each tank was evenly floored with eight conditioned ceramic tiles and eight unconditioned tiles in a 4 × 4 checkered patterns. The unconditioned tiles were lack of biofilm. The experiment lasted 60 days in a shade shed at 25.07 ± 2.64 °C (mean ± SD), maintained by a chiller set to 25 °C, under a natural light-dark cycle, with a light level of approximately 150 µmol photons m^{-2} s^{-1} during the light period.

2.1.3 Measurements on larval settlement & growth

The settlement numbers of larvae on both conditioned and unconditioned tiles were documented on day 0 and day 60, with measurements of tissue area changes conducted under a digital camera, following methodologies similar to those outlined in previous research (Naumann et al., 2009). Image capture was facilitated by a digital camera (Canon 200d: 24.2 megapixels resolution) in combination with a macro lens (Laowa 90mm f/2.8 2x Ultra Macro APO) and a speed flash (Godox TT685II). Each image was captured vertically, with tiles fully submerged in filtered seawater and a scale in proximity for accurate image scaling. Subsequent image processing occurred with ImageJ software (v1.53t). Calibration of photo scale was achieved utilizing the straight line tool and Set scale function, converting into pixel dimensions. The polygon tool was employed at a 100% zoom level to outline the perimeter of each larva. The measure function within the software was then used to calculate the surface area (mm^2) of the coral larvae based on the encircled area.

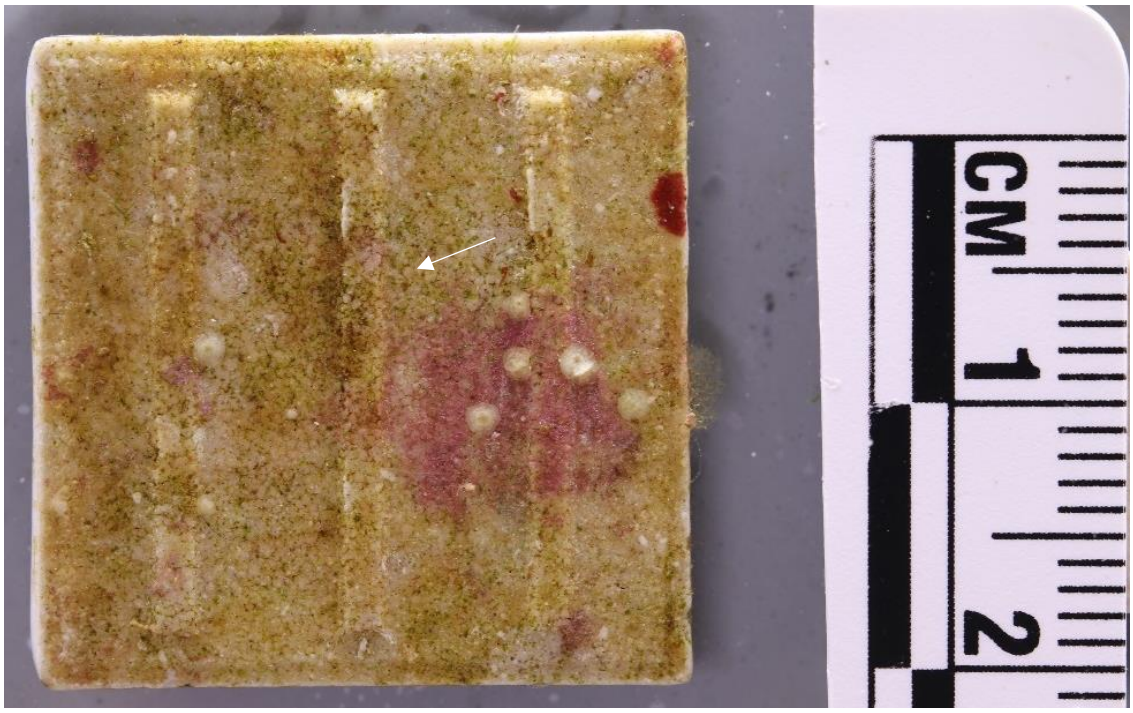

Figure 2. 4 Images of the tile, inclusive of a scale for reference, were captured using a digital camera (canon 200d: resolution 24.2 megapixels) in combination with a macro lens (Laowa 90mm f/2.8 2x Ultra Macro APO) and a speed flash (Godox TT685II). The settled coral larvae are denoted by a white arrow in the image.

2.1.4 Measurements on microplastic ingestion

The settled larvae were fixed by formaldehyde solution (4%) and stored in PBS (1x, pH 7.4) at four degrees Celsius. Samples were later observed for microplastic ingestion under Eclipse Ti2-E live-cell imaging system (Nikon, Japan). Under the microscope, the larval samples were excited at 385nm laser and observed through multiband filter set (DAPI/FITC/TRITC/Cy5). The fluorescence of coral tissue, zooxanthellae and fluorescent PS particles could be distinguished through the fluorescence microscope. Ingested microplastics by *A. tumida*, if any, located within the coral gastrovascular cavity were recorded.

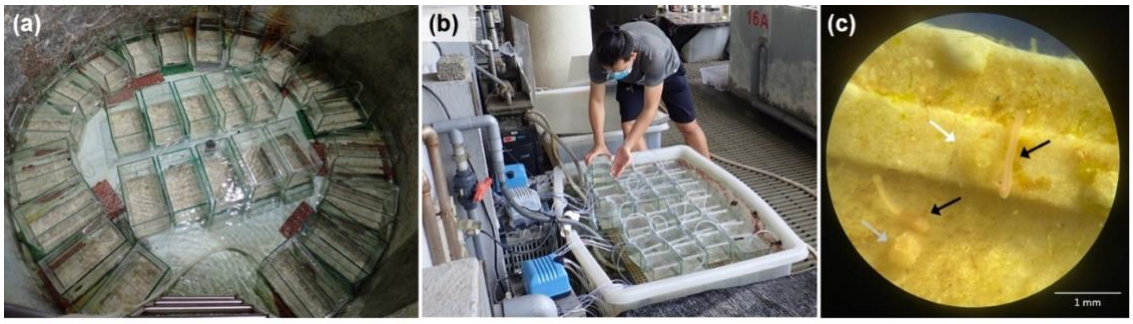

Figure 2. 5 (a) Part of the hatchery facilities used in this project to produce coral larvae of *A. tumida* for **(b)** the experimental setup; **(c)** stereomicrograph showing planula larvae (black arrowed), a settling larva (grey arrowed) and a settled larva (white arrowed).

2.2 Juvenile and Adult Coral Responses to Microplastics and Sediments

2.2.1 Samples collection

The *A. tumida* larvae were collected by scuba divers and cultured in Simon F.S. Li Marine Science Laboratory for 12 months until experiment use. The recruit of branching coral *Acropora tumida* were served as the test species since they are the major broadcast-spawning corals in Hong Kong and were available for collection during the study period. Fragments of adult *A. tumida* collected from the field (about 40 mm height; Fig. 2.7). The juvenile and adult of *A. tumida* were served as the test species in this study since they are the major broadcast-spawning corals in Hong Kong and were available for collection during the study period.

2.2.2 Treatments preparation

Two types of microplastics were tested, including naturally buoyant polypropylene (PP; density = 0.85–0.92 g cm^{-3}) and negatively buoyant polyethylene terephthalate (PET; density = 1.16–1.41 g cm^{-3}), both of which are common in Hong Kong waters (Leung et al., 2021; Lo et al., 2018). Microplastics of PP and PET were produced from domestic plastic products with a Retsch CryoMill (Haan, Germany; see Fig. 2.6). Natural sediment used in the experiment was collected from the Tung Ping Chau Marine Park and subsequently heated in an oven at 500 °C for one hour to eliminate potential environmental microplastics, before being dried (Fig. 2.2 a). The particles of PP, PET and sediment were sieved to a size range of 50–106 μm.

The experiments comprised four treatments, namely control treatment, PP treatment (10 mg L^{-1}), PET treatment (10 mg L^{-1}), and sediment treatment (10 mg L^{-1}), for juvenile *A. tumida* with 15 replicates distributed in 3 tanks (1 L) per treatment, and for adult *A. tumida* with 15 replicates distributed in 5 tanks (1 L) per treatment. The control treatment contained no dosed particles. The other three treatments tested the effects of PP, PET and sediment particles on *A. tumida*. Each replicate tank contained 1 L of filtered seawater at 35 ‰ salinity, of which flow was maintained by aeration. A 150μl of homogenised *Artemia* was added in each treatment on day 0. The experiment lasted 30 days in a shade shed at 25.98 ± 2.00 °C (mean ± SD), maintained by a chiller set to 25 °C, under a natural light-dark cycle, at about 150 μmol photons m^{-2} s^{-1} during the light period. The treatment media and *Artemia* were renewed every 3 days.

2.2.3 Measurements on growth, photosynthesis and bleaching

At the start and end of the exposure experiment, the samples of juvenile and adult *A. tumida* were assessed with a Maxi Imaging-PAM chlorophyll fluorometer (Walz, Germany) to determine three photosynthesis-related parameters of zooxanthellae within the coral tissue, namely the minimum fluorescence yield (Fo), absorptivity (Abs) and maximum quantum yield of photosystem II (Fv/Fm, described in Fig. 2.7). Growth of juvenile *A. tumida* was reflected on the size change in tissue area measured under a stereomicroscope with the ImageJ software (Schneider et al., 2012). Growth of adult *A. tumida* was indicated by the change in buoyant weight following the method of Fang et al. (2013). Bleaching of juvenile and adult corals were monitored by grey scale photos taken by a stereomicroscope and a digital camera and analysed by ImageJ.

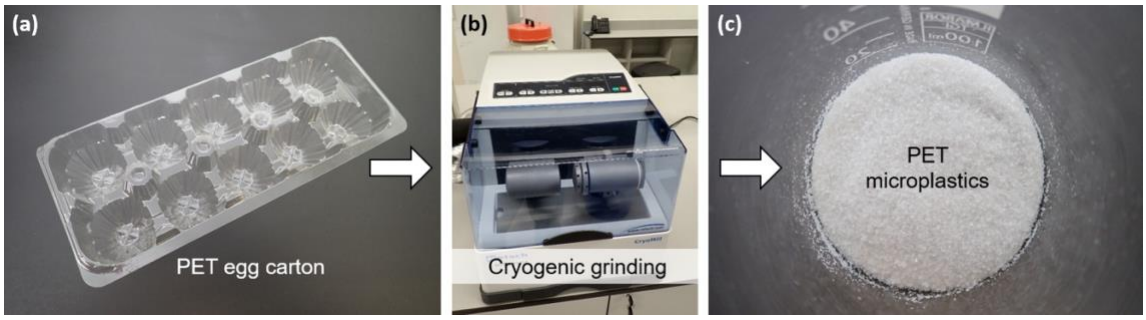

Figure 2. 6 Preparation of microplastics. (a) Plastic egg carton represents a common domestic waste of polyethylene terephthalate (PET) and (b) were cryogenically ground at –196 °C using a Retsch CryoMill (Haan, Germany) to produce (c) plastic particles of PET for the experiments. Likewise, microplastics of polypropylene (PP) were prepared from the same batch of disposable PP cups using the CryoMill.

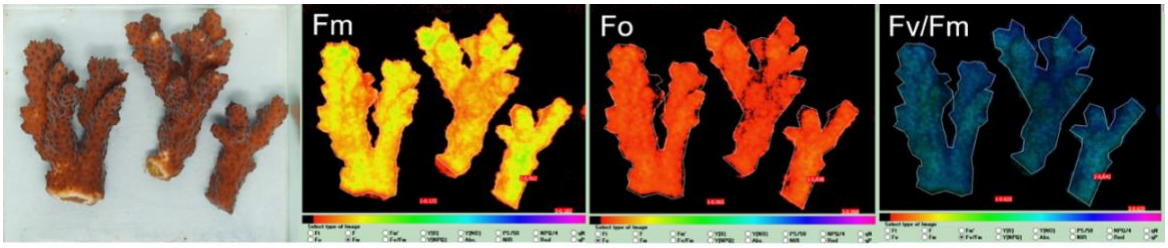

Figure 2. 7 Coral fragments of *A. tumida* and assessed with a Maxi Imaging-PAM chlorophyll fluorometer (Walz, Germany). Photosynthesis-related parameters were measured, including maximum and minimum fluorescence yields (Fm and Fo, respectively, indicating the maximum light harvesting capacity and relative amount of chlorophyll a), and maximum quantum yield of photosystem II (Fv/Fm, representing the efficiency to process captured photons for photosynthesis). Absorptivity (Abs), another indicator of the relative amount of chlorophyll a, was also measured. Relative values are displayed using an identical colour scale, which ranges from 0 (black) to 1 (purple) as shown at the bottom. Juvenile *A. tumida* was assessed using the same method.

2.3 Microplastics in Corals and Habitats in Mirs Bay

2.3.1 Samples collection

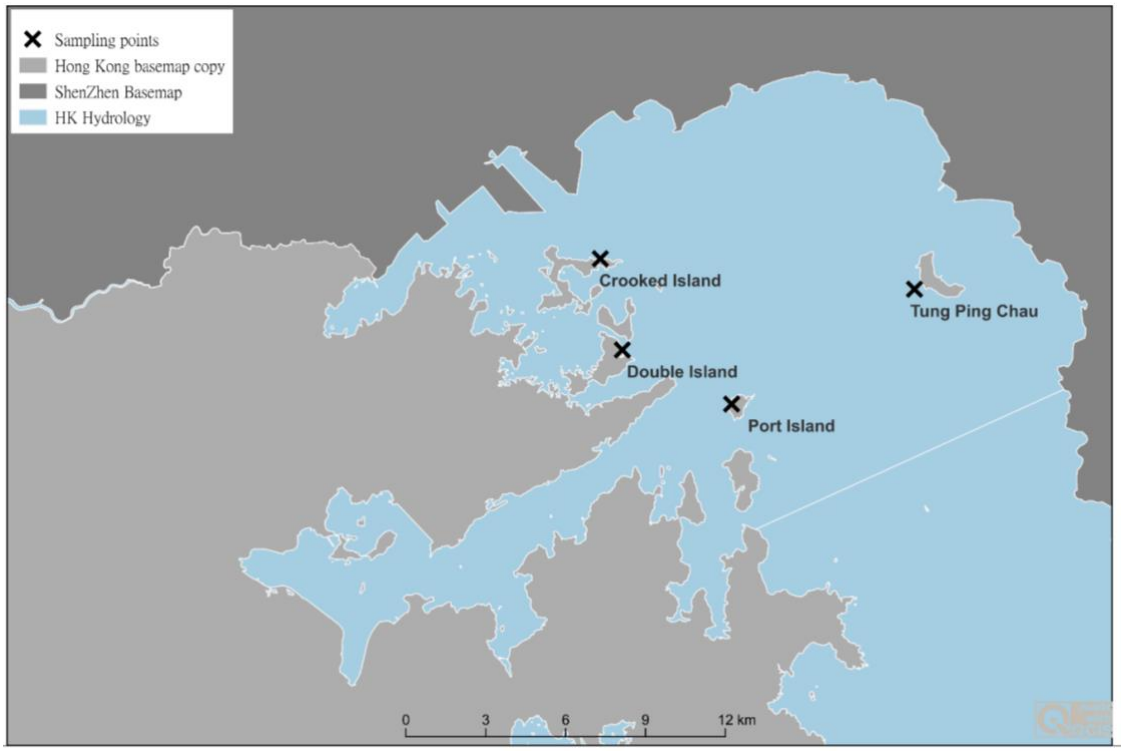

Figure 2. 8 QGIS map of Mirs Bay indicating the sampling sites of *Platygyra acuta*. Areas shaded in grey and dark grey represent Hong Kong and Shenzhen, respectively, while blue denotes hydrology. The locations of the four sampling sites are marked with crosses.

Samples were collected from Crooked Island (CI), Double Island (DI), Port Island (PI), and Tung Ping Chau Marine Park (TPC) in Mirs Bay. CI, DI, and PI are situated in the west, surrounded by densely populated residential areas, while TPC is in the east, characterized by sparsely populated rural regions. CI, DI, and PI are affected by the development of East Hong Kong and South Shenzhen, where construction and human activities are ongoing. Additionally, CI and DI are proximate to the Yantian International Container Terminal. TPC, however, is farther from Hong Kong and adjacent to the rural lands of Shenzhen, implying lower pollution levels.

Samples, including coral fragments and adjacent sediments, were collected from these sites. All samples were retrieved by scuba divers using 12 cm × 5 cm × 10 cm fish tanks with covers that had been washed with 1% nitric acid. Collected samples were then stored at the Simon F.S. Li Marine Science Laboratory and the Hong Kong Polytechnic University for experimental

use. The collected coral species, *Platygyra acuta* (Fig. 2.1 a), served as the test species in this study, as it is one of the major broadcast-spawning corals in Hong Kong and was available for collection during the study period. This species is a dominant, aggressive and more heterotrophic coral species in Hong Kong reef communities (Tsang & Ang, 2019).

Pairs of *P. acuta* fragments and adjacent sediments were collected between 2020 and 2021 from Crooked Island and Double Island in March (spring season), Port Island in January (winter season), and Tung Ping Chau Marine Park in September (summer season). All samples were collected by scuba divers using 12 cm × 5 cm × 10 cm fish tanks with covers that had been washed with 1% nitric acid. During each collection, five coral samples were placed in zip bags and stored on ice baths, while five sediment samples were wrapped in aluminium foil. Samples were then transported to the laboratory and stored in a −20 °C freezer at the Simon F.S. Li Marine Science Laboratory, and later at the Hong Kong Polytechnic University, for experimental use. The collected coral fragments were "corals of opportunity," dislodged coral fragments that would not have survived otherwise. Sample collection in the Tung Ping Chau Marine Park was conducted with permission from the Agriculture, Fisheries and Conservation Department, Government of the Hong Kong SAR (permit number: 51 in AF MPD 09/3 Pt.24).

2.3.2 Microplastics extraction procedure

Sediment digestion protocol

Each sample of dried sediment (500 g) was mixed with one litre of sodium iodide solution (density = 1.70 g cm^{-3}) in a two-litre beaker (Lo et al., 2018). The mixture was stirred at 120 rpm for ten minutes using an overhead stirrer (LC-OES-200SH, Lichen). Two cycles of sedimentation and filtration followed. In each cycle, the beaker was covered with aluminium foil and stored in a cabinet to allow sedimentation for one day. The supernatant was then filtered through 31 µm stainless steel filters using a vacuum pump. The stainless-steel filters containing trapped particles were transferred to a 400 ml beaker, and 150 ml of digestive solution (1% KOH; 5% EDTA; 5% H_2O_2) was added. The mixture was sonicated for ten minutes. The filters were then washed with Milli-Q water and removed from the solution. Particles were retrieved from the solution onto a 31 µm stainless steel filter via vacuum filtration. The particles were then ready for polymer identification.

Soft tissue digestion protocol

This digestion procedure was modified from Leung et al. (2021). Coral fragments were briefly washed with Milli-Q water to remove adhered sediment, followed by digestion in a one-litre beaker containing a solution of potassium hydroxide (KOH, 10%) and hydrogen peroxide (H_2O_2, 3.5%), mixed on a shaker at 70 rpm. After three days, coral tissue was solubilized by digestion. The undigested coral skeleton was removed from the solution, and adhered particles on the skeleton were washed back into the one litre beaker. Ethylenediaminetetraacetic acid disodium salt dihydrate (EDTA, 10%) was added to dissolve adhered sediments over one day. The supernatant was filtered through a 31 µm stainless steel filter using a vacuum pump, while the precipitate was centrifuged (C-28A, BOECO Germany) in 50 ml Falcon tubes at 2500 rpm for five minutes. The supernatant was filtered using the 31 µm stainless steel filter, and the precipitate, after adding Milli-Q water, was subjected to another round of centrifugation. The remnant underwent density separation using sodium iodide (NaI, 1.7 g/ml) to a total volume of 40 ml, with two cycles of sonication for ten minutes and centrifugation at 2500 rpm for five minutes. In each cycle, the supernatant containing lighter particles was filtered through a 31 µm stainless steel filter using a vacuum pump. Particles retained on the filter were then subjected to microplastic identification.

Coral skeletons digestion protocol

After soft tissue digestion, the remaining skeletons were sonicated with Milli-Q water and dried in an oven at 40 °C. Dry skeletons were weighed and scanned using a 3D camera to measure mass, surface area, and volume. The samples were then digested using 5.5% hydrochloric acid (HCl) with minimal volume at 40 °C. The pH of the liquefied skeleton solution was adjusted to 10–11 using 20% KOH solution. Hydrogen peroxide solution (30%) was added to reach a 5% concentration, added four times at twelve-hour intervals, to aid in the digestion of skeletal organic matter. If whitish precipitates appeared during pH adjustment, EDTA (10%) was added until dissolution. The solution was then left to sediment for 24 hours. The supernatant containing lighter particles was filtered through a 31 µm stainless steel filter using a vacuum pump. The remnant underwent density separation using sodium iodide (NaI, 1.7 g/ml) to a total volume of 40 ml, with two cycles of sonication for ten minutes and centrifugation at 2500 rpm for five minutes. In each cycle, the supernatant containing lighter particles was filtered through

the 31 μm stainless steel filter using a vacuum pump. Particles retained on the stainless-steel filters were then subjected to microplastic identification.

2.3.3 Microplastics identification

Particles (>31 μm) extracted from the coral soft tissue, coral skeleton, and sediment samples were collected on stainless-steel filter membranes and identified using a Renishaw inVia confocal Raman microscope (Wotton-under-Edge, UK; see Leung et al. 2021a, 2021b; Ho et al. 2022). The microscope system was coupled with a Leica 10× objective (Wetzlar, Germany) and a 785 nm edge laser (300 mW output power). The system included an automated mapping mode, which aided the identification process and produced data for particle quantification, polymer type identification, and particle size distribution.

Particles retained on the stainless-steel filter were scanned at a spatial resolution (pixel size) of 28.4 μm and excited by the laser at 10% power for 5 s per pixel. Approximately 14,000 Raman spectra were generated for each sample during the automatic 2D scan (mapping). Baseline correction and cosmic ray removal of the spectra were performed using Renishaw WiRE 5.2 software. The refined Raman spectra were matched with the Renishaw Polymeric Materials Database for polymer identification. Each pixel (28.4 μm) was scored for similarity compared to the standard spectra in the database. The matching index ranged from 0.00 to 1.00, with higher values representing greater similarity. For matching indices >0.7, the matching was accepted. For indices between 0.4 and 0.7, the spectra were examined visually to determine if the sample spectra consisted of all the signature peaks of the standard spectra in the database. Otherwise, the matching was rejected. The accepted matching of a pixel was color-coded to indicate the detection of a polymer in the software.

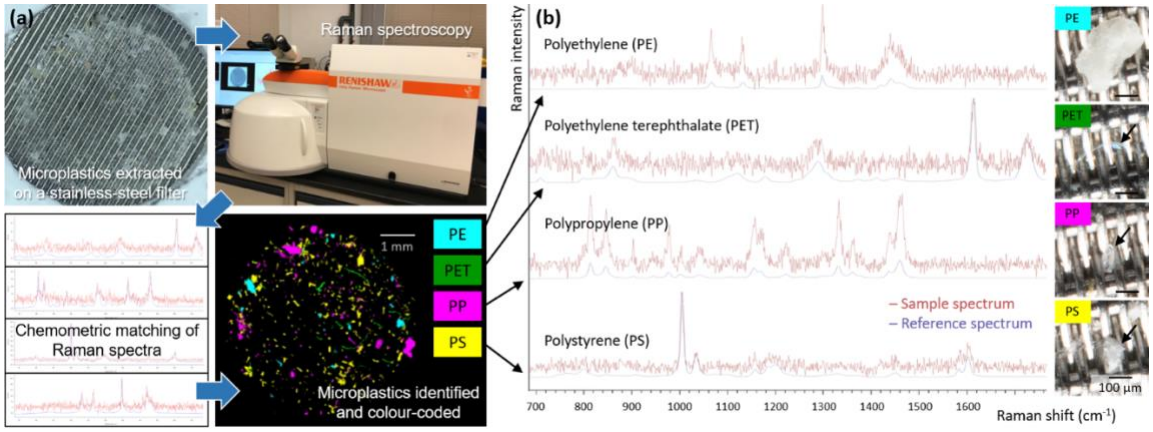

Figure 2. 9 The workflow for analyzing microplastics in the laboratory using a Renishaw inVia confocal Raman microscope (Wotton-under-Edge, UK; see Ho et al. 2022); (b) Examples of microplastics identified from the coral and sediment samples in Part III and their Raman spectra compared to the reference spectra.

2.3.4 Three dimensions scanning of coral fragments

Skeleton samples were scanned (Fig. 2.10) using an EinScan Pro 2X handheld 3D scanner (Shining 3D, China) to obtain 3D data, which were processed by Geomagic Design X 2022 software for repairing, hole filling, and global remeshing. In brief, corals were rotated on a disc and captured at different angles. The generated models were remeshed with a resolution of 0.2 mm.

Figure 2. 10 (a) The University Research Facility in 3D Printing (U3DP) at The Hong Kong Polytechnic University, where (b) fragments of *P. acuta* were scanned using an EinScan Pro 2X handheld 3D scanner (Shining 3D, China) to determine the tissue surface area.

2.4 Statistical Analyses

2.4.1 Statistical Framework and Model Specification

All analyses were conducted within a Bayesian statistical framework using generalised linear mixed-effects models (GLMMs) implemented in the *brms* package (version 3.4.1) in R (Bürkner, 2017). Bayesian methods provide several advantages over traditional frequentist approaches in handling small or noisy datasets, including enhanced reliability, greater accuracy, and the ability to explicitly incorporate prior knowledge (Kruschke et al., 2012; van de Schoot et al., 2021). Bayesian results offer direct probabilistic interpretations, which facilitate clear inference regarding effect presence and magnitude (Kruschke, 2010).

Numeric continuous variables were z-standardised (mean = 0, SD = 1) prior to analysis to enhance interpretability and sampling efficiency (Schielzeth, 2010), and multicollinearity was not detected. Weakly regularising priors (mean = 0, SD = 1) were applied to all fixed and random effects, balancing model flexibility with conservative shrinkage to minimise the risk of overfitting. Models were fitted using four Markov Chain Monte Carlo (MCMC) chains, each comprising 2,000 iterations with 1,000 warm-up steps, resulting in a total of 4,000 post-warm-up posterior samples. All models demonstrated satisfactory convergence, with Rhat values $\leq$ 1.01, effective sample sizes exceeding 1,000, and no divergent transitions or convergence issues identified (Cowles & Carlin, 1996).

Credible intervals (CI) were used to assess effect sizes, analogous to frequentist confidence intervals but interpreted probabilistically. The 89% CI, which has long been recommended as the default in *bayestestR* (Makowski et al., 2019), is generally more stable for estimation (Kruschke, 2015), while the 95% CI aligns more closely with the conventional frequentist threshold and provides a more conservative standard (e.g., $p = 0.05$). In this study, effects were categorised as follows:

1) Strong/significant evidence: 95% CI excluded zero.
2) Moderate evidence: 89% CI excluded zero, but 95% CI overlapped zero.
3) No evidence: Both 89% and 95% CI included zero.

This dual-threshold approach enhanced analytical transparency, distinguishing practical relevance (89% CI) from stricter statistical significance (95% CI), while avoiding overinterpretation of borderline effects.

2.4.2 Experiment-Specific Model Structures

Impacts of MPs on corals at the larval stage

For the larval experiment, settlement rates were analysed using a binomial GLMM with a logit-link function. The response variable represented the number of larvae settled out of 100 per tank (event-trial format). Growth rate was analysed using a Gaussian GLMM with an identity-link function. Fixed effects comprised treatment (Control, Zx, PS, Mix), tile substrate condition (conditioned vs. unconditioned), and their interaction. A random intercept for tank accounted for non-independence among replicates within treatment groups.

To quantify the relative contribution of treatments and substrate conditions in explaining larval settlement and growth variability, fixed-effect coefficients were converted into variance components (Nakagawa et al., 2013). The proportion of variance explained by each component was calculated through dividing its variance estimate by the total model variance, including fixed, random, and residual variance components.

Impacts of MPs on Juvenile and Adult Corals

For the juvenile and adult coral experiments, variables such as growth and photochemical performance were analysed using Bayesian GLMM. Gaussian models with identity-link functions were applied to continuous values. Fixed effects included treatment (four levels: Control, PP, PET, and sediment). Initial Day 0 measurements were added as covariates to adjust for baseline differences and were z-standardised (mean = 0, standard deviation = 1) prior to analysis. A random intercept for tank was incorporated to account for within-group dependency.

Effect size interpretation integrated both 89% and 95% CI with the Region of Practical Equivalence (ROPE) methodology. ROPE evaluates the proportion of posterior distribution

falling within a predefined null range (±0.1 for standardised parameters). low percentages indicate meaningful effects and high percentages support null effects. ROPE boundaries followed Cohen's (1988) guidelines for negligible effect sizes (Kruschke & Liddell, 2018). Following Bayesian methodological conventions, 89% CI highest density intervals (HDIs) were prioritised for ROPE evaluations due to their favourable statistical properties compared to 95% intervals, as implemented in the bayestestR package (Kruschke, 2015; Kruschke & Liddell, 2018; Makowski et al., 2019; McElreath, 2016). Complementing this, the probability of direction (PD) metric provided additional evidence strength, indicating the certainty of an effect's sign (50% = complete uncertainty, 100% = absolute certainty), analogous to one-tailed frequentist p-values (Makowski et al., 2019).

Monitoring MPs in Coral Habitats

For the field-based MPs analysis in coral habitats, MPs concentrations (items cm^{-3}) were analysed using Bayesian zero-inflated beta GLMM to account for overdispersion, residual non-normality (despite log transformation) and true zeros arising from biological absence. Separate models were constructed for total MPs and each major polymer type (PE, PET, PP, PS), while rarer polymers (e.g., nylon, PTFE, PVC, PMMA) were excluded due to low detection frequencies. Fixed effects included site (four levels: Crooked Island, Double Island, Port Island, and Tung Ping Chau), sample type (coral skeleton vs. sediment), and their interaction. Random intercepts were included to account for spatial pseudo-replication across sampling points within each site and seasonal variability associated with field campaigns.

Chapter 3 – Results

3.1 Larval Settlement and Growth

3.1.1 Overview of settlement rate and growth rate

Tile conditioning exerted a pronounced influence on larval settlement, whereas treatment-related differences were limited (Fig. 3.1 A). On conditioned tiles, the proportion of larvae that settled was highest in the Control (34.70%), followed by Zx (30.00%) and PS (29.70%). The Mix treatment, however, resulted in lowest attachment (23.00 %). In contrast, on unconditioned tiles, attachment success declined sharply across all treatments (control = 1.67 %; Zx = 7.00 %; Mix = 6.00 %; PS = 2.33 %).

Growth showed little variation among treatments (Fig. 3.1 B). Under conditioned tiles, mean growth clustered around the reference value (98.51 – 102.57 %), while unconditioned tiles produced a modest increase (103.52 – 106.76 %), with no clear treatment pattern.

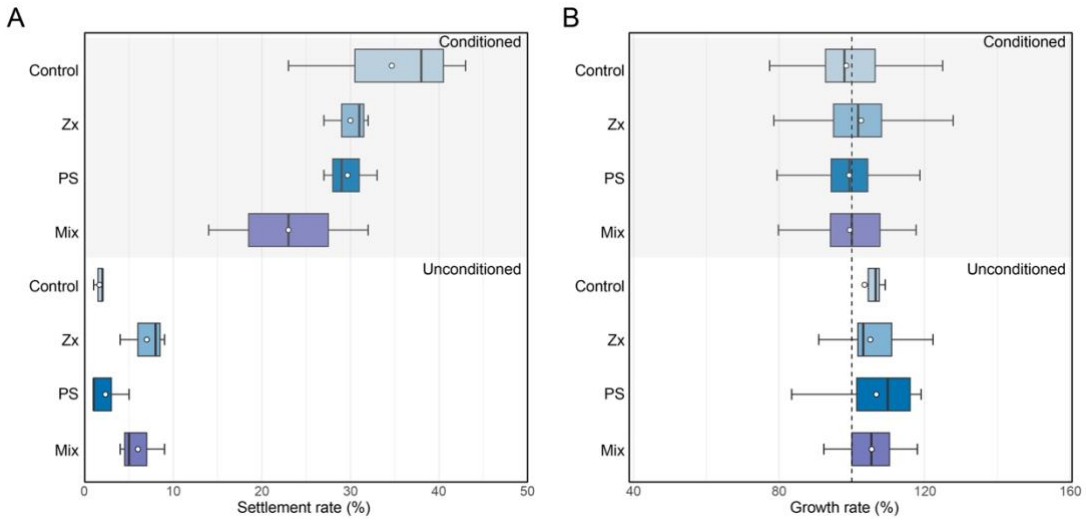

Figure 3. 1 Settlement and growth of *A. tumida* larvae after 60 days. white dots = mean; lines = median; boxes = interquartile range (IQR); whiskers = data spread; dashed vertical line = 100 %, the reference value.

3.1.2 Bayesian Posterior Modelling

The Bayesian GLMM for settlement explained 87 % of the variance (R^2 = 0.87, Fig. 3.2 A). Relative to the control on conditioned tiles, the Mix treatment showed strong evidence of ≈ 38 % settlement reduction (posterior median log-odds, % [credible interval]: –0.46, 95% CI [0.81, –0.12]). In contrast, effects of Zx and PS were minimal (Zx: –0.11, 95% CI [-0.44, 0.22]; PS: –0.15, 95% CI [-0.48, 0.20]). Unconditioned tiles imposed a substantial decline in larval attachment (–2.72, 95% CI [–3.31, –2.16), although this was partially offset by positive interactions with Zx (0.89, 95% CI [0.15, 1.65]) and Mix (1.06, 95% CI [0.34, 1.82]). The growth model carried little explanatory power (conditional R^2 = 0.09; Fig. 3.2b). All main and interaction effects were not significant in growth. Posterior diagnostics confirmed full model convergence (Rhat = 1.00) and adequate sampling efficiency (bulk ESS > 1,500).

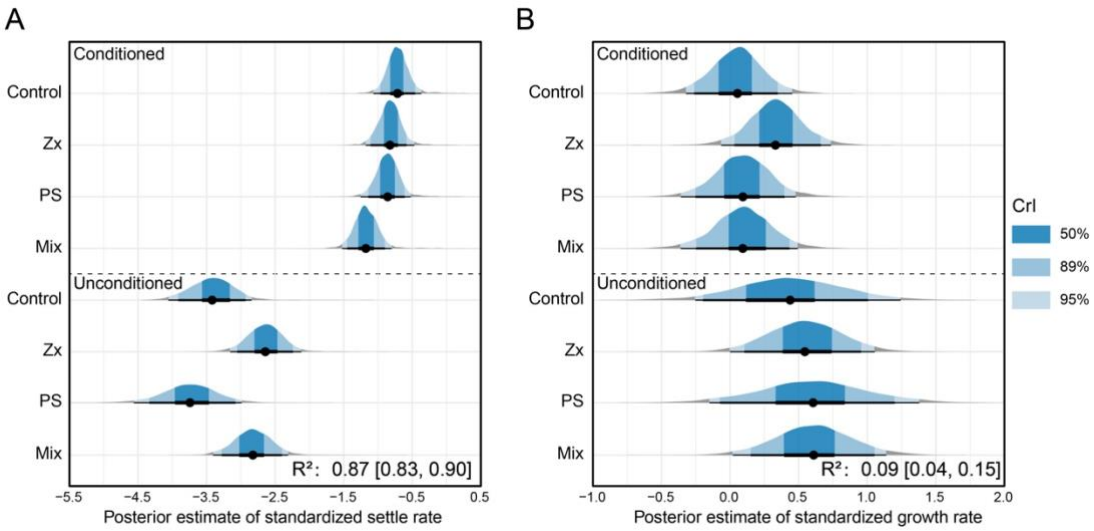

Figure 3. 2 Bayesian GLMM Posterior estimates and credible intervals for standardized settlement (A) and growth (B). Dots = medians; Lines = 50%, 89% and 95% CI. Dashed line separates tile conditions. Posterior R^2 values indicates model explanatory power.

3.1.3 Bayesian Hypothesis Testing

Posterior pairwise contrasts, used as Bayesian analogues to post-hoc tests, quantified differences among treatment × tile combinations (Fig. 3.3).

On conditioned tiles, the Mix treatment reduced settlement rate relative to the control (–0.46, 95% CI [–0.81, –0.12]), whereas Zx and PS showed no significant effects. Pairwise comparisons confirmed moderate evidence (89% CI) for reduced settlement in Mix compared with either Zx or PS, while differences between Zx and PS were negligible.

On unconditioned tiles, settlement was consistently suppressed (95% CI) across all treatment. In this context, Zx significantly improved larval performance (0.89, 95% CI [0.15, 1.65]), and Mix showed moderate evidence of a positive effect (1.06, 89% CI [0.34, 1.82]). PS did not differ from the control group. Direct comparisons indicated a significant positive effect of Zx over PS (95% CI). Transitioning from conditioned to unconditioned tiles led to a universal and significant reduction in settlement (95% CI), underscoring the dominant influence of substrate conditioning.

Neither main effects nor interaction effects were significant for larval growth, with all 89% & 95% CIs overlapping zero. However, there was moderate evidence (89%) that Mix increased growth rate on unconditioned tiles compared with conditioned tiles, suggesting a tile-dependent response (Fig.3.3).3).

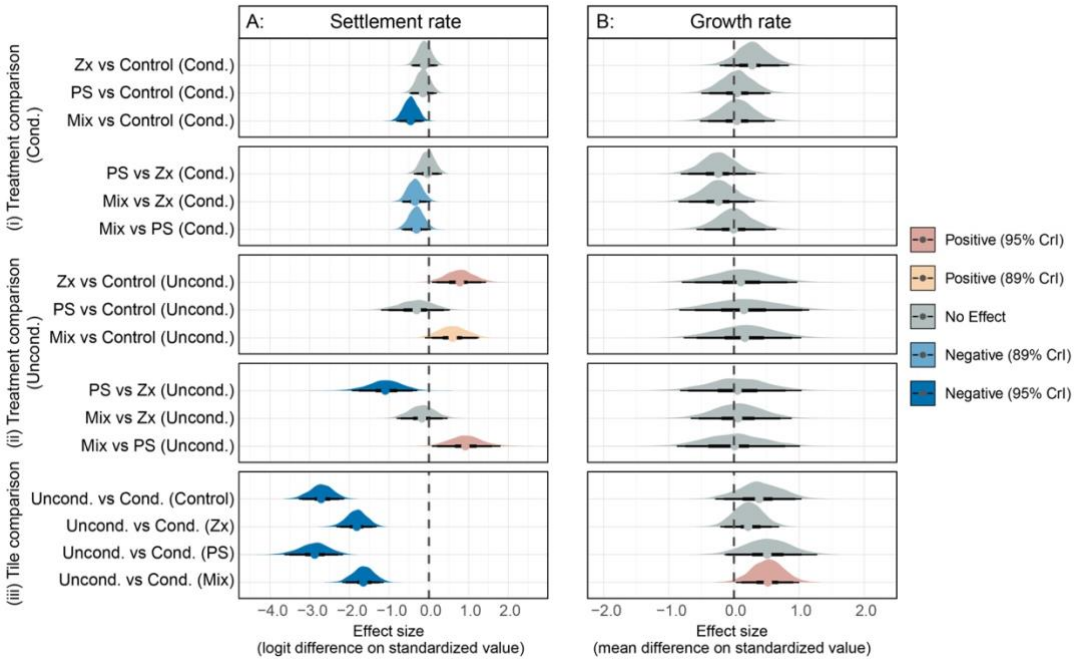

Figure 3. 3 Posterior estimates for standardised settlement (A) and growth (B) across treatments and tile conditions. Density plots show effect size between treatment pairs: i) within conditioned tiles, ii) within unconditioned tiles, iii) across tile conditions; lines (50 %, 89 % & 95 % CI); colour (red = positive, blue = negative, grey = non-significant). Estimates are based on standardised model outputs.

3.1.4 Variance Decomposition

The variance explained analysis revealed distinct patterns in how settlement and growth rates were influenced by experimental factors. For settlement rate (Fig. 3.4 A), substrate conditioning (tiles) explained the largest variance (median = 19%, 95% CI [13%, 25%]). Treatment effects contributed minimally, while the interaction effect of treatment and tile condition exerted modestly, reflecting influences under unconditioned conditions.

In contrast, the variance in growth rate distributed evenly (Fig. 3.4B) with treatment (0% – 16%), tiles (0% – 10%) and their interaction (0% – 8%). The distribution indicates neither treatment nor substrate conditioning strongly determined growth. Random effects, such as tank identity and microenvironmental variation, likely dominated growth outcomes. The result suggests uncontrolled background heterogeneity plays a dominant role in growth outcomes.

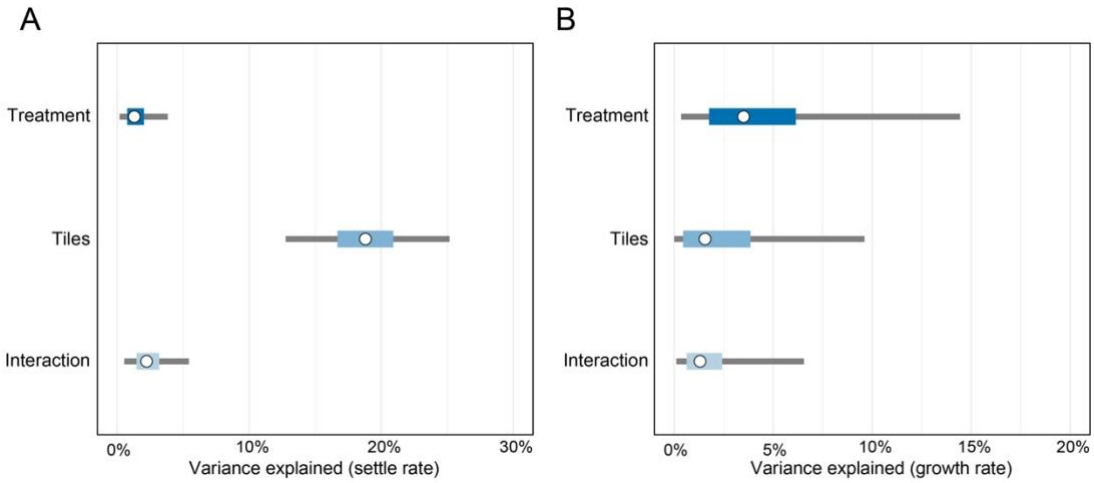

Figure 3. 4 Variance decomposition for larval responses: Settlement rate (A) and growth rate (B). Percentage scales show contributions from treatment, tile condition, and interactions. Dots = medians variance proportions; bars = IQR; lines = 95% CI. Percentage scales show contributions from treatment, tile condition, and interactions.

3.1.5 MPs ingestion

Coral larvae ingested MPs in the experiment. However, only less than 5% of *A. tumida* larvae were found ingesting the PS particles in the PS and Zx + PS treatments of the experiment, according to observation reported in Fig. 3.5.

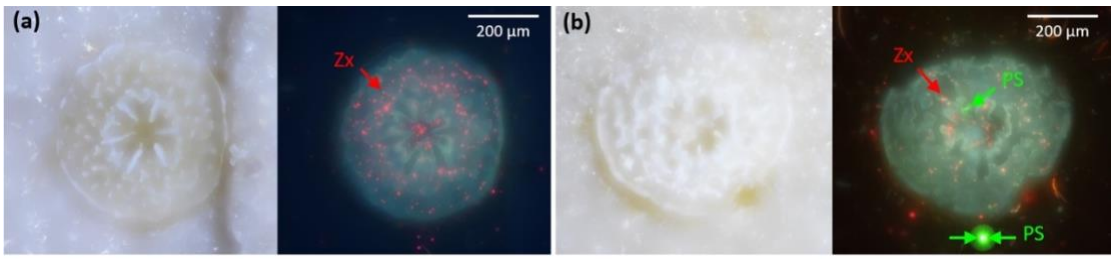

Figure 3. 5 Zooxanthellae (Zx; *Symbiodinium clade C1*) inoculation in larvae under different conditions. Fluorescent micrographs show normal symbiont uptake without MPs (A) and simultaneous incorporation of PS particles (10 µm) during symbiont acquisition (B). Images were captured using a Nikon Eclipse Ti2-E live-cell imaging system, demonstrating PS internalization by the coral host.

3.2 Growth and Photosynthesis of Juvenile and Adult Corals

3.2.1 Effects of MPs and sediment on the growth capability of juvenile *A. tumida*

Exposure to MPs and sediment affected juvenile *A. tumida* growth, as indicated by changes in surface area and polyp count over 30 days. Surface area was highest in the control group (mean = 139.2%), followed by sediment (138.5%) and PET (130.4%) treatments, while PP-treated corals exhibited the lowest mean value (117.7%) (Fig. 3.6 A). Polyp numbers showed a similar trend, with the highest count in the PP group (63.3), followed by Control (61.8), sediment (59.9), and PET (56.6) (Fig. 3.6 B).

Bayesian posterior estimates further support treatment-specific effects. The Bayesian R^2 values indicated that the models explained a substantial proportion of variance in growth responses: $R^2 = 0.69$ (95% [0.59, 0.76]) for surface area, and $R^2 = 0.71$ (95% [0.62, 0.77]) for polyp count (Fig. 3.7). For surface area (Table 3.1), PP exposure was associated with a potential reduction in growth. The 89% CI (-0.93, -0.01), low ROPE overlap (4.69%) and a 94.78% probability of direction (PD) indicate a biologically meaningful effect. However, the 95% CI (-1.06, 0.11) overlapped zero. In contrast, PET and sediment treatments had a negligible effect on surface area, indicated by CI overlapping zero. For polyp counts (Fig. 3.7 B and Table 3.1), PP and sediment both led to reductions compared to the control group. PP treatment shows strong evidence (89% CI [-1.06, -0.11]; 89% ROPE = 0%; 95% CI [-1.18, 0.03]; PD = 97%) and sediment yielding slightly weaker but consistent results (89% CI [-0.87, -0.05]; 89% ROPE = 2.98%; 95% CI [-0.99, 0.06]; PD = 96.2%). PET effects on polyp count were less clear, with moderate posterior support. Collectively, these results highlight PP as the most detrimental treatment to coral surface growth and polyp density.

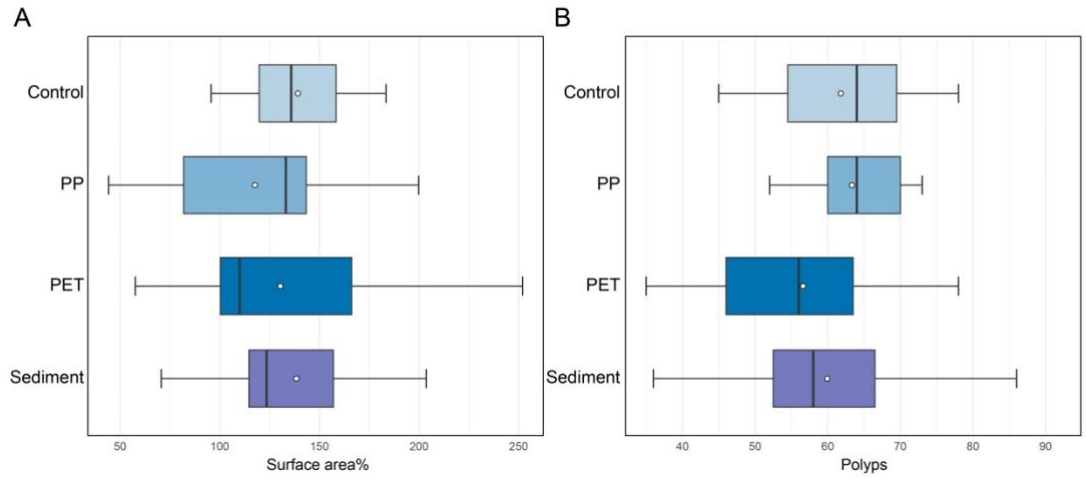

Figure 3. 6 Morphological responses of juvenile corals to MPs exposure. Surface area (A) and polyp count (B) are shown across treatments (Control, PP, PET, Sediment). White dots = means; lines = median; Boxes = IQR; whiskers = data spread.

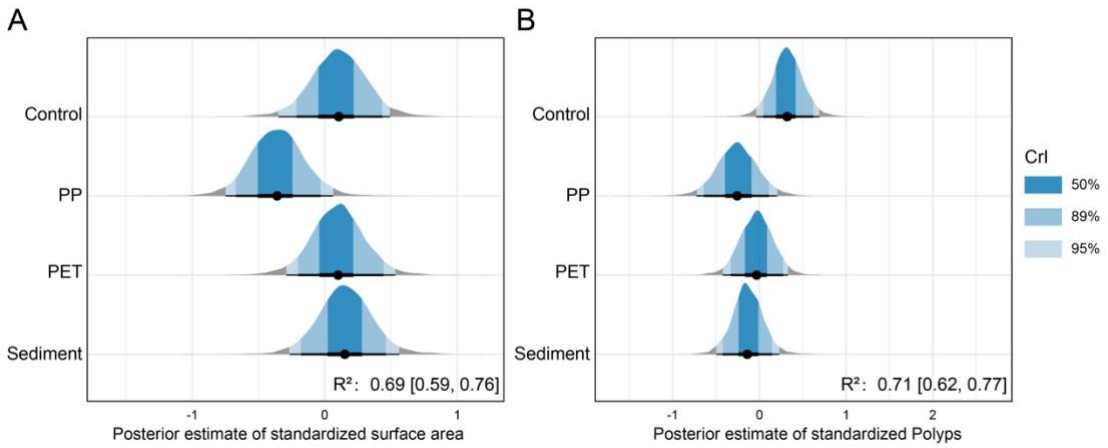

Figure 3. 7 Bayesian GLMM posterior distributions of MPs and sediment exposure on juvenile coral growth. Standardised surface area (a) and polyp count (b) are presented for treatments (Control, PP, PET, Sediment). Black dots = medians; lines = 50%, 89% & 95% CI; R^2 indicates model explanatory power.

Model	Parameter	89% CI	89% ROPE	95% CI	95% ROPE	PD
Surface area	PP	[-0.93, -0.01]	4.69	[-1.06,0.11]	7.29	94.78
	PET	[-0.46,0.45]	32.64	[-0.57,0.57]	30.58	51.15
	Sediment	[-0.43,0.51]	30.79	[-0.55,0.64]	28.84	56.98
Polyps	PP	[-1.06, -0.11]	0	[-1.18,0.03]	3.11	97
	PET	[-0.77, 0.05]	10.93	[-0.9,0.15]	12.13	91.85
	Sediment	[-0.87, -0.05]	2.98	[-0.99,0.06]	5.95	96.2

Table 3. 1 Summary of Bayesian model estimates for juvenile *A. tumida* growth capability relative to control group. The table shows the 89% and 95% CI, percentage of the posterior distribution within the Region of Practical Equivalence (ROPE; ±0.1), and the probability of direction (PD). Lower ROPE and higher PD values suggest more meaningful treatment effects.

Bayesian pairwise comparisons revealed treatment-specific differences in both coral surface area and polyp number. For surface area (Fig. 3.8 A), the contrast between PP and Control showed moderate evidence (89% CI) of growth inhibition. Comparisons between PP and both PET and sediment also suggested negative shifts in posterior distributions with moderate support (89%). In contrast, PET and sediment treatments showed little difference from Control with CI overlapping zero. For polyp count (Fig. 3.8 B), all treatments had posterior estimates suggesting lower values relative to the Control, particularly for PP and sediment with moderate evidence (89% CI). Comparisons between treatments yielded minimal evidence for difference in posterior distribution.

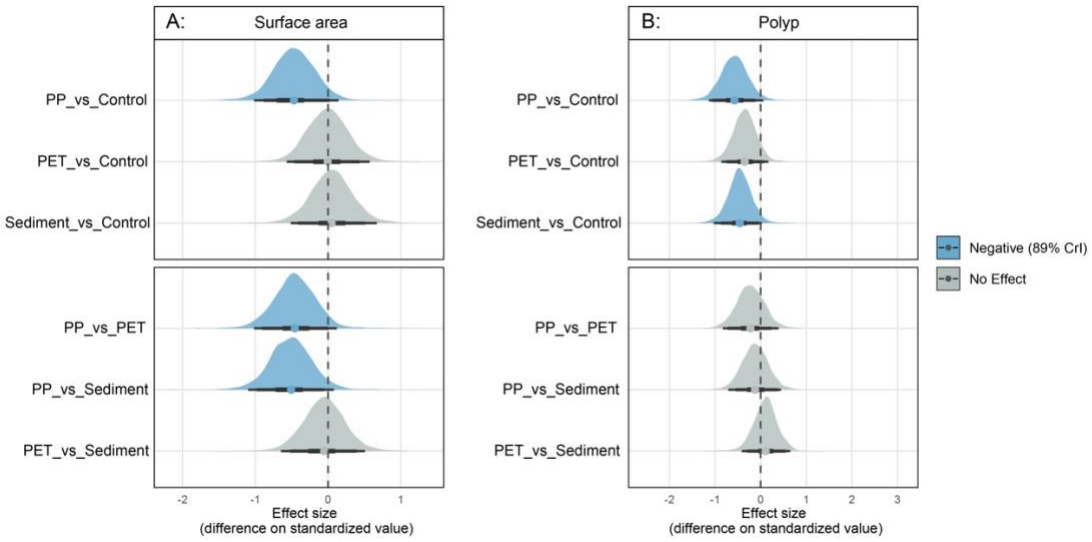

Figure 3. 8 Posterior estimates and hypothesis testing of juvenile coral growth under MP and sediment exposure. Standardised surface area (A) and polyp count (B) are shown across treatments (Control, PP, PET, Sediment). Density plots display effect sizes; lines = 50%, 89% and 95% CI; colours (blue = negative, red = positive, grey = non-significant) indicate statistical support. Estimates are based on standardised model outputs.

3.2.2 Effects of MPs and sediment on the photochemical performance of zooxanthellae in juvenile *A. tumida*

Exposure to MPs and sediment induced treatment-specific variation in the photochemical performance of zooxanthellae in juvenile *A. tumida*, as reflected on grey scale, Abs, Fo, and Fv/Fm (Figs. 3.9-3.10; 3. 2). Grey scale values were highest in PP treatment (mean = 151.2), indicating potential pigment loss. Control and PET treatments showed lower values (107.8 and 108.8, respectively). Bayesian models supported a detectable increase in brightness under PP treatment, with a positively shifted posterior distribution (89% ROPE = 1.15%, PD = 94.98%). The effects of PET and sediment were more uncertain. The model explained 51.2% of the variance in grey scale ($R^2 = 0.51$, 95% CI [0.35, 0.63]). Abs, the lowest values were observed in the PP group (0.833) while PET and sediment treatments (0.880 and 0.881) showed higher means. PP exposure was associated with a negatively shifted posterior (89% ROPE = 3.37%, PD = 93.2%), indicating a likely reduction in photosynthetic absorption, with model $R^2 = 0.57$ (95% CI [0.41, 0.67]). Fo peaked under PET (0.0565), followed by Control (0.0536), and was lowest under PP (0.0435). Bayesian estimates revealed a pronounced decline in Fo under PP exposure (95% ROPE = 0.97%, PD = 97.33%) while PET and sediment effects were less

certain. The model explained 40% of variance in Fo (R^2 = 0.40, 95% CI [0.22, 0.55]). Finally, Fv/Fm was highest in the control (0.702) and declined slightly in PET treatment (0.701). The lowest values were in the PP (0.664) and sediment (0.701) treatments. PP exposure again produced a negatively shifted posterior (89% ROPE = 3.82%, PD = 93.08%). The model for Fv/Fm had the highest explanatory power (R^2 = 0.60, 95% CI [0.45, 0.69]).

Bayesian pairwise comparisons revealed treatment-specific differences in photochemical performance among juvenile *A. tumida*. For grey scale values (Fig. 3.11 A), PP showed positive contrasts relative to the control group (89% CI excludes 0), suggesting increased tissue brightness. The PP and PET comparison also positively shifted (89% CI excludes 0). In contrast, PP exposure was consistently associated with reduced values for Abs (Fig. 3.11 B) compared to PET (89% CI excludes 0) and sediment (95% CI excludes 0), indicated by negatively shifted posterior distributions. These results align with the model-based posterior estimates suggesting lower photosynthetic absorption under PP treatment. For Fo (Fig. 3.11 C), PP was lower than control group (89% CI excludes 0). No meaningful pairwise differences were detected for Fv/Fm (Fig. 3.11 D) because all contrasts showed posterior distributions broadly overlapping zero.

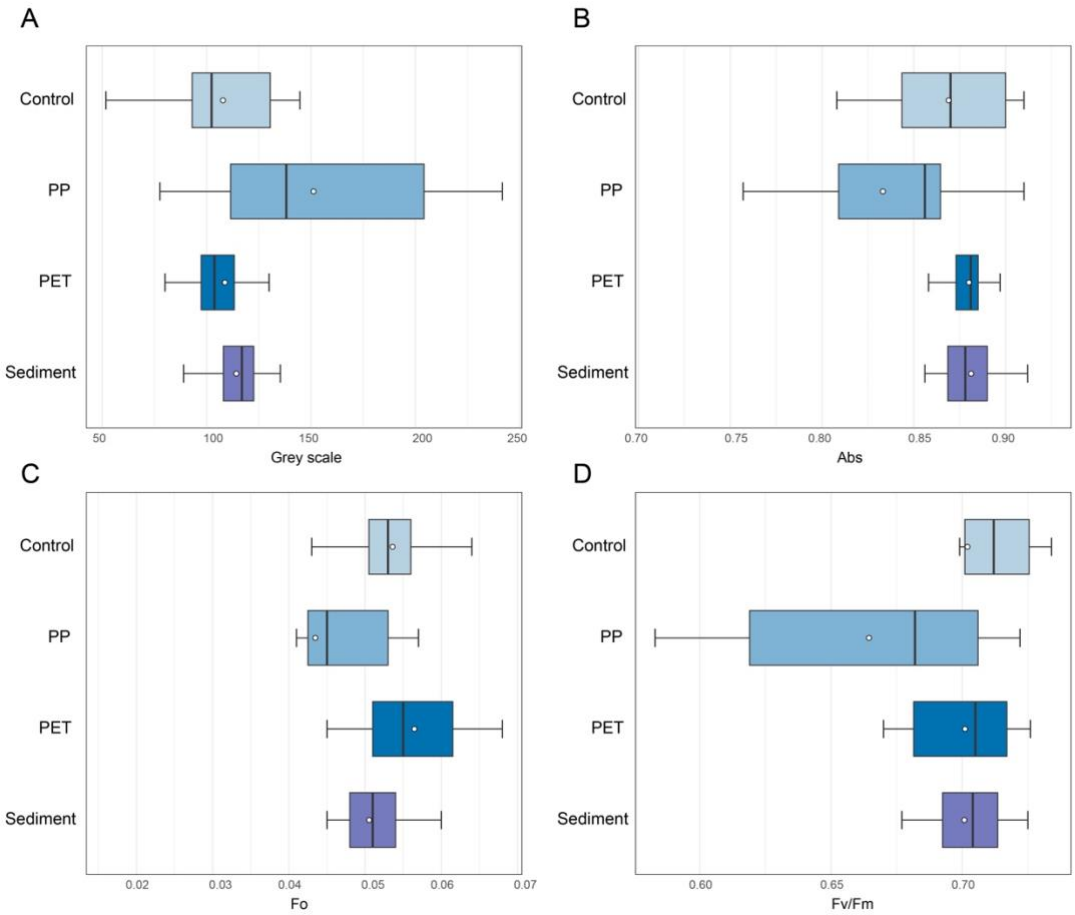

Figure 3. 9 Photochemical responses of zooxanthellae in juvenile corals following exposure to MPs and sediment. Grey scale (A), Abs (B), Fo (C), and Fv/Fm (D) are shown across treatments (Control, PP, PET, Sediment). Dots = means; Lines = medians; Boxes= IQR; whiskers = data spread.

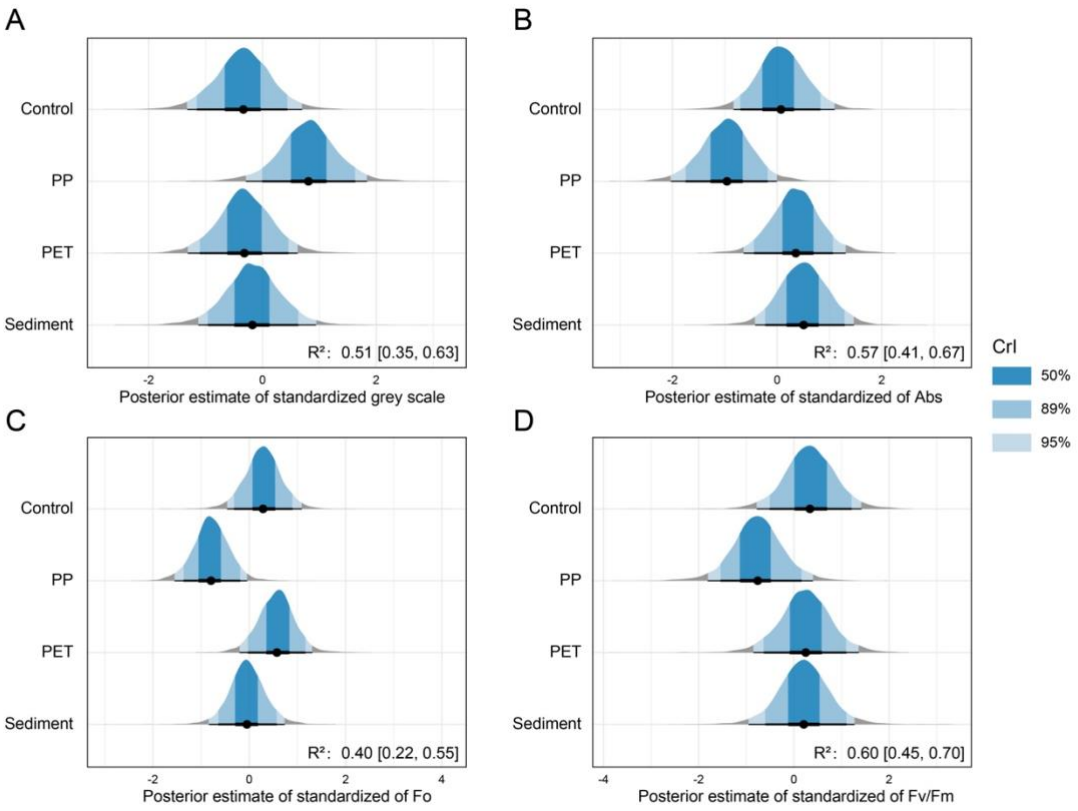

Figure 3. 10 Bayesian GLMM posterior distributions and CI of photochemical performance of juvenile corals exposed to MPs and sediment. Standardised grey scale (A), Abs (B), Fo (C), and Fv/Fm (D) are shown across treatments (Control, PP, PET, Sediment). Dots = medians, and lines = 50%, 89%, and 95% CI. Posterior R^2 values indicate model explanatory power.

Model	Parameter	89% CI	89% ROPE	95% CI	95% ROPE	PD
Greyscale	PP	[0.04,2.3]	1.15	[-0.28,2.6]	2.61	94.98
	PET	[-1.08,1.16]	14.35	[-1.37,1.42]	13.45	52.18
	Sediment	[-0.95,1.28]	11.97	[-1.2,1.61]	11.21	59.53
Abs	PP	[-2.18,0.08]	3.37	[-2.48,0.38]	3.34	93.2
	PET	[-0.83,1.4]	12.16	[-1.17,1.7]	11.39	67.6
	Sediment	[-0.63,1.52]	11.12	[-0.89,1.82]	10.42	74.63
Fo	PP	[-1.89,-0.26]	0	[-2.14,0.03]	0.97	97.33
	PET	[-0.57,1.12]	14.94	[-0.84,1.36]	14	72.03
	Sediment	[-1.18,0.54]	14.55	[-1.38,0.77]	13.63	74.2
Fv/Fm	PP	[-2.31,0.08]	3.82	[-2.67,0.43]	3.76	93.08
	PET	[-1.25,1.11]	12.25	[-1.62,1.42]	11.47	56.35
	Sediment	[-1.36,1.1]	11.94	[-1.68,1.46]	11.18	57

Table 3. 2 Summary of Bayesian model estimates for the photochemical performance of zooxanthellae in juvenile *A. tumida* relative to control group. The table shows the 89% and 95% CI, percentage of the posterior distribution within the Region of Practical Equivalence (ROPE; ±0.1), and the probability of direction (PD). Lower ROPE and higher PD values suggest more meaningful treatment effects.

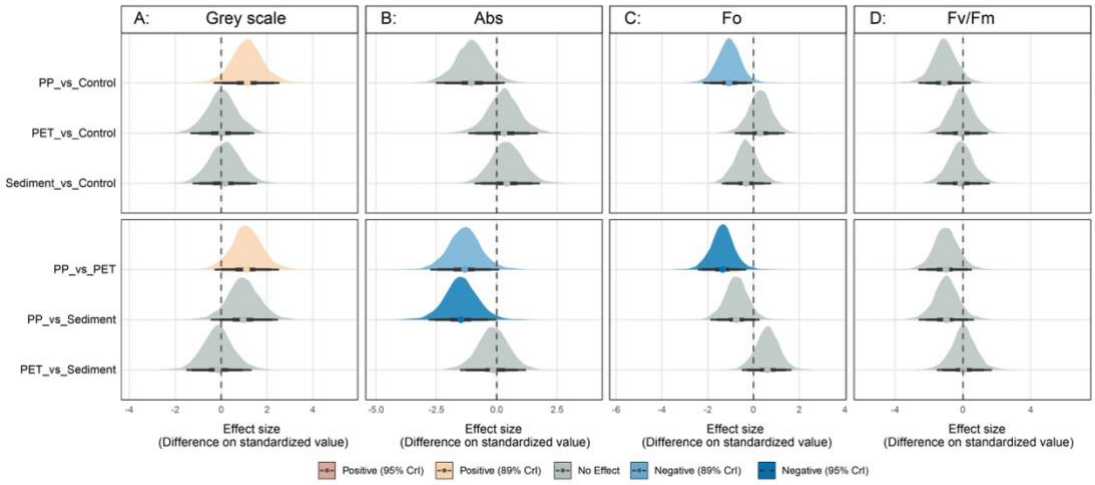

Figure 3. 11 Posterior estimates of photochemical responses in juvenile corals exposed to MPs and sediment. Standardised grey scale (A), Abs (B), Fo (C), and Fv/Fm (D) are shown across treatments (Control, PP, PET, Sediment). Density plots represent the effect size between treatments; line = 50%, 89%& 95% CI and colours (blue=negative, red=positive, grey=non-significant) indicate statistical support. Estimates are based on standardised model outputs.

3.2.3 Effects of MPs and sediment on the growth capability of adult *A. tumida*

by changes in buoyant weight over 30 days (Fig. 3.12). Observed buoyant weight was highest in the PET group, with comparable mean values across Control, PP, and sediment treatments (Fig. 3.12 A). Bayesian models supported this observation as all treatment posterior estimates showed extensive overlap and narrow variation around the control (Fig. 3.12 B). The model demonstrated strong explanatory power (R^2 = 0.99, 95% CI [0.99, 0.99]). At the parameter level (Table 3.3), none of the treatments showed credible effects on buoyant weight. All CIs (89% & 95%) overlapped zero, ROPE overlap was 100%, and PD remained below conventional thresholds of confidence. Pairwise comparisons among treatments and relative to the control further confirmed negligible differences, with all posterior distributions were near zero and overlapping CI (Fig. 3.13).

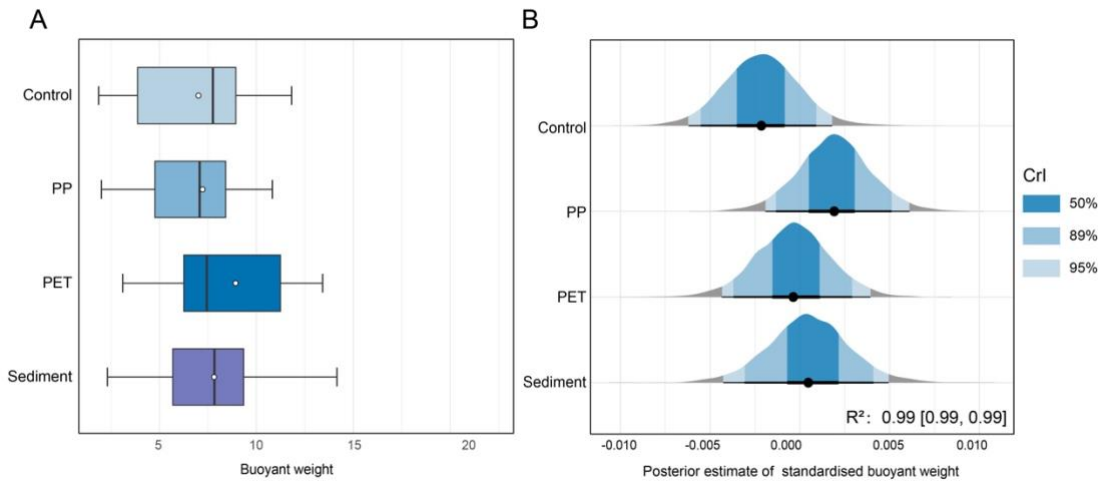

Figure 3. 12 Observed and modelled buoyant weight of adult corals following exposure to MPs and sediment. (A) Boxplots show observed buoyant weights. Dots = means; lines = medians; Boxes = IQR; whiskers = data spread. (B) Bayesian GLMM posterior distributions and CI of standardized buoyant weight. Dots = medians, and lines = 50%, 89% & 95% CI. Posterior R^2 values indicate model explanatory power.

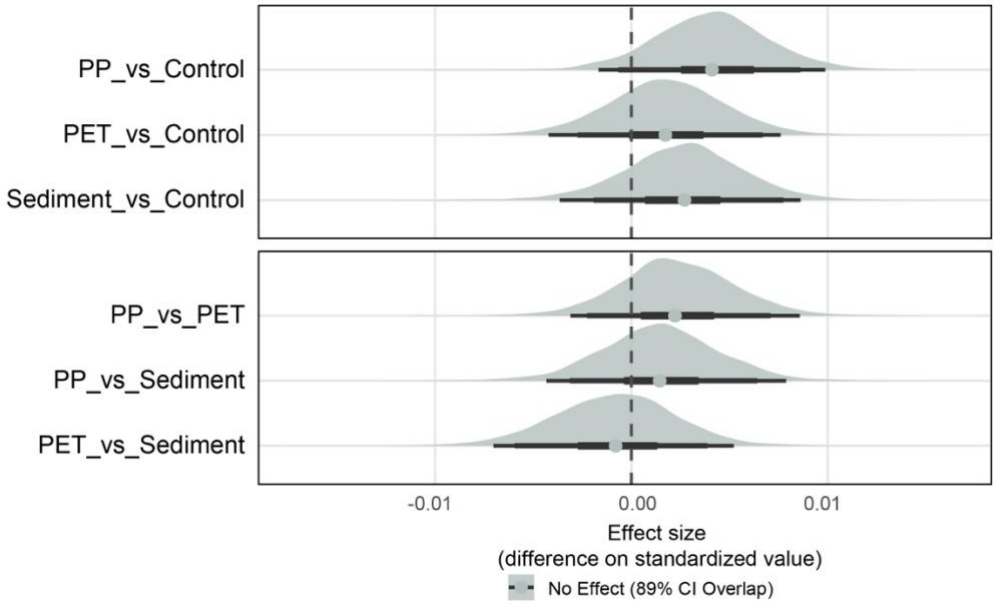

Figure 3. 13 Posterior estimates and hypothesis testing of adult corals growth under MPs and sediment exposure. Density plots represent the effect size between treatments. Lines = 50%, 89% & 95% CI. colours (blue=negative, red=positive, grey=non-significant) indicate statistical support. Estimates are based on standardised model outputs.

Model	Parameter	89% CI	89% ROPE	95% CI	95% ROPE	PD
Buoyant	PP	[-0.001,0.009]	100	[-0.002,0.01]	100	92.38
weight	PET	[-0.003,0.006]	100	[-0.004,0.008]	100	73.38
	Sediment	[-0.002,0.007]	100	[-0.004,0.009]	100	81.98

Table 3. 3 Summary of Bayesian model estimates for adult *A. tumida* growth capability (buoyant weight) relative to control group. The table shows the 89% and 95% CI, percentage of the posterior distribution within the Region of Practical Equivalence (ROPE; ±0.1), and the probability of direction (PD). Lower ROPE and higher PD values suggest more meaningful treatment effects.

3.2.4 Effects of MPs and sediment on the photochemical performance of zooxanthellae in adult *A. tumida*

Exposure to MPs and sediment exerted limited effects on the photochemical performance in adult *A. tumida* (Fig. 3.14 - 3.15). Bayesian models revealed moderate explanatory power for grey scale (R^2 = 0.53, 95% CI [0.35, 0.66]), Fo (R^2 = 0.53, 95% CI [0.31, 0.66]) and Fv/Fm (R^2 = 0.53, 95% CI [0.34, 0.66]), but weak explanatory capacity for Abs (R^2 = 0.22, 95% CI [0.05, 0.41]).

Across all the parameters, posterior distributions showed CI (89% & 95%) overlapping zero, high ROPE percentages (typically >10–15%), and low PD for most treatments. For instance, grey scale values under PP and PET exposures showed ROPE overlaps (15.4–16.5%) and low PD (55%), suggesting negligible effect on coral pigmentation. Sediment exposure produced a more positively shifted posterior in grey scale (PD = 86.6%), yet this effect remained inconclusive due to overlapping CI on zero. Similarly, Abs values remained broadly stable across treatments, with ROPE overlaps (16% – 18%), and significant directional certainty across treatments. Fo showed a potentially positive effect under sediment exposure (ROPE = 5.03%, PD = 90.7%), but this was not supported due to overlapping of CI on zero. Effects on Fv/Fm followed a similar pattern, with overlapping posterior distributions and weak support for treatment-specific change (Table 3.4).

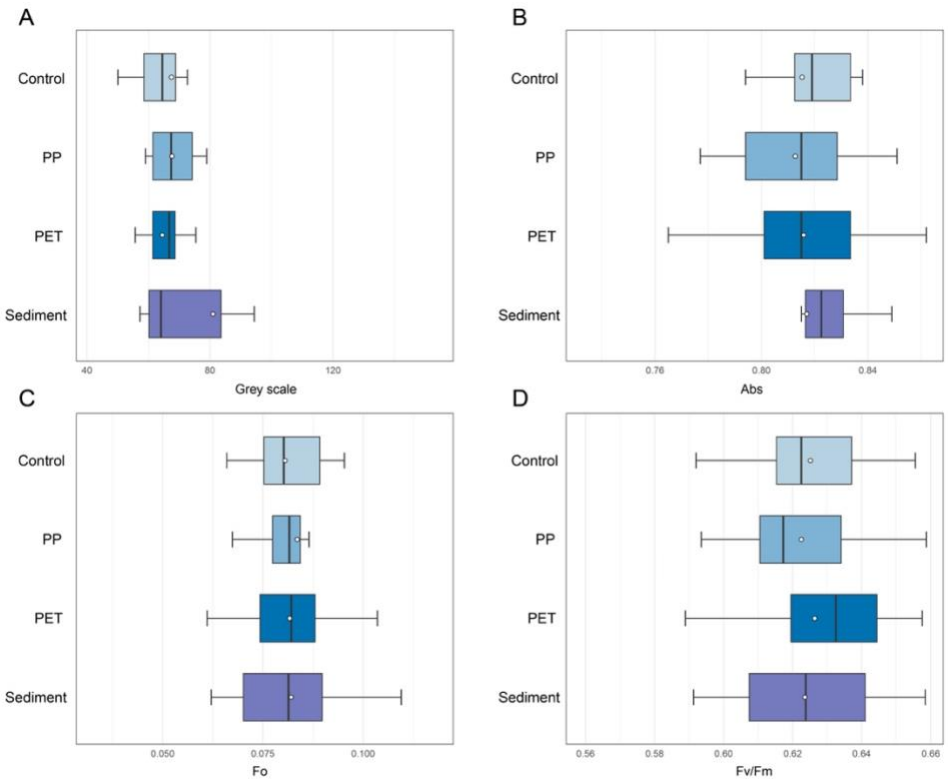

Figure 3. 14 Photochemical responses of zooxanthellae in adult corals following exposure to MPs and sediment. Grey scale (A), Abs (B), Fo (C), and Fv/Fm (D) are shown across treatments (Control, PP, PET, Sediment). Dots = means; Boxes = IQR; lines = medians; whiskers = data spread.

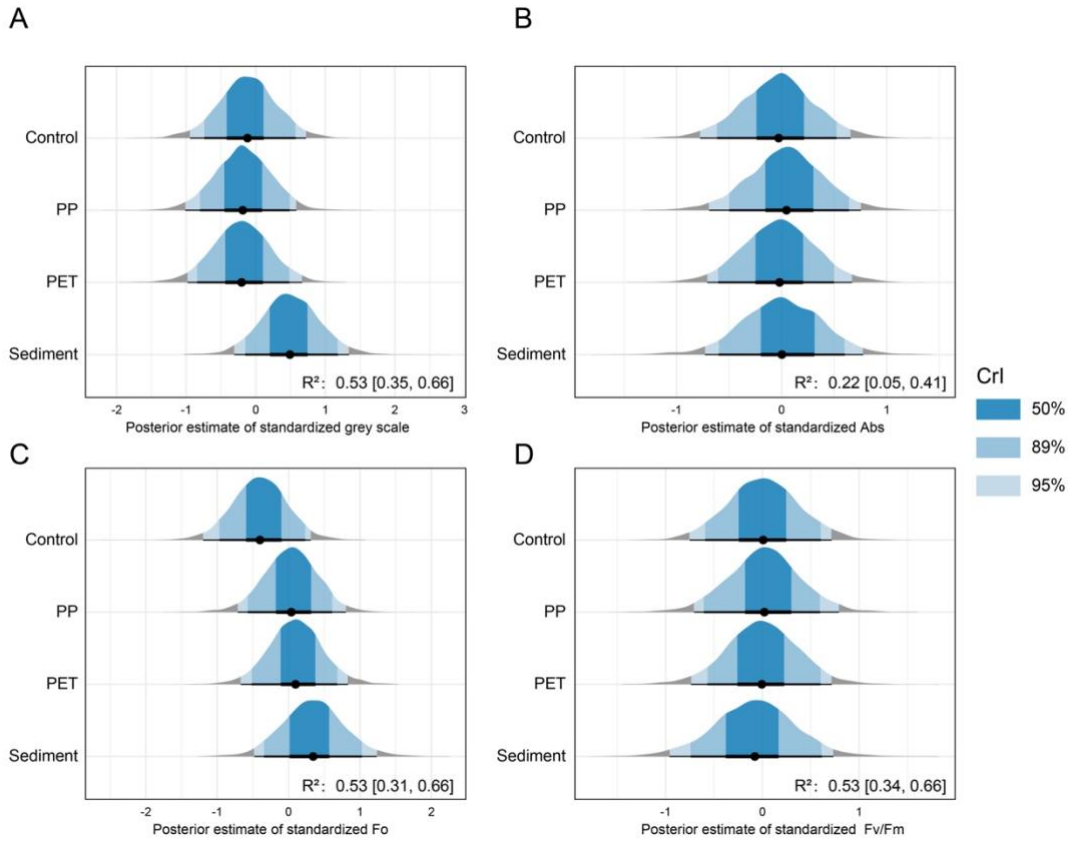

Figure 3. 15 Bayesian GLMM posterior distributions and CI of photochemical responses in zooxanthellae in adult corals following exposure to MPs and sediment. Standardised grey scale (A), Abs (B), Fo (C), and Fv/Fm (D) are shown across treatments (Control, PP, PET, Sediment). Dots = medians, and lines = 50%, 89% & 95% CI. Posterior R^2 values indicate model explanatory power.

Model	Parameter	89% CI	89% ROPE	95% CI	95% ROPE	PD
Greyscale	PP	[-0.97,0.83]	16.49	[-1.19,1.05]	15.45	54.88
	PET	[-1.05,0.85]	15.42	[-1.29,1.11]	14.45	55.98
	Sediment	[-0.27,1.54]	8.06	[-0.5,1.76]	7.55	86.6
Abs	PP	[-0.76,0.91]	17.33	[-0.97,1.13]	16.24	55.73
	PET	[-0.79,0.8]	19.66	[-1,0.99]	18.42	50.95
	Sediment	[-0.81,0.87]	17.72	[-1,1.09]	16.61	53.08
Fo	PP	[-0.42,1.28]	11.77	[-0.63,1.5]	11.03	79.73
	PET	[-0.34,1.38]	10.79	[-0.55,1.63]	10.11	83
	Sediment	[-0.17,1.71]	5.37	[-0.39,1.94]	5.03	90.7
Fv/Fm	PP	[-0.82,0.86]	17.11	[-1.02,1.05]	16.03	50.98
	PET	[-0.86,0.81]	18.2	[-1.1,1.02]	17.05	51.48
	Sediment	[-0.99,0.79]	15.9	[-1.18,1.01]	14.89	56.88

Table 3. 4 Summary of Bayesian model estimates for the photochemical performance of zooxanthellae in adult *A. tumida* relative to control group. The table shows the 89% and 95% CI, percentage of the posterior distribution within the Region of Practical Equivalence (ROPE; ±0.1), and the probability of direction (PD). Lower ROPE and higher PD values suggest more meaningful treatment effects.

Pairwise Bayesian comparisons further supported the lack of statistically meaningful effects on the photochemical performance of zooxanthellae in adult *A. tumida* (Fig. 16). Across all contrasts, the 89% CI overlapped zero, and none of the comparisons yielded credible evidence for biologically relevant shifts. These findings collectively suggest that the photochemical performance of zooxanthellae in adult *A. tumida* are resilient to short-term MPs and sediment exposure. No consistent impairment was observed in their photochemical functioning.

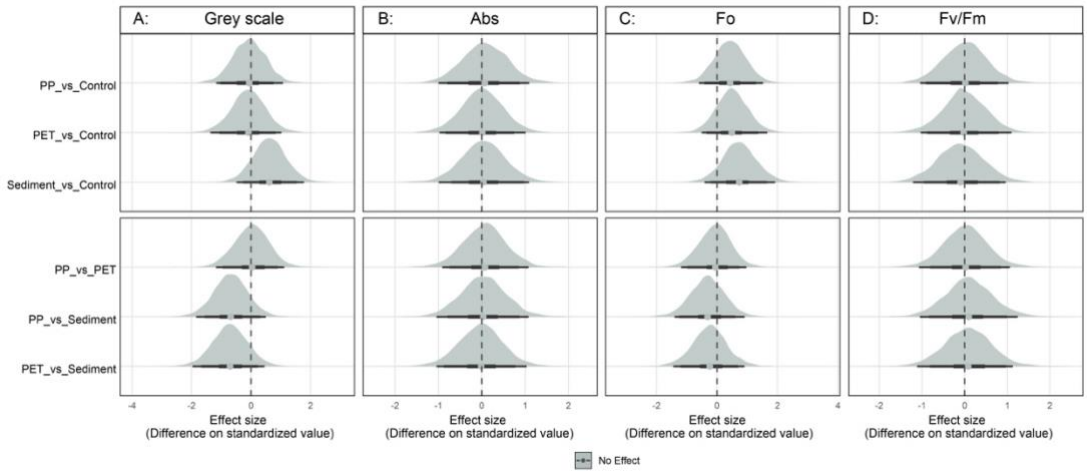

Figure 3. 16 Posterior estimates and hypothesis testing of photochemical responses in zooxanthellae in adult corals under MPs and sediment exposure. Standardised grey scale (A), Abs (B), Fo (C), and Fv/Fm (D) are shown across treatments (Control, PP, PET, Sediment). Density plots represent the effect size between treatments. Lines = 50%, 89% & 95% CIs and colours (blue=negative, red=positive, grey=non-significant) indicate statistical support. Estimates are based on standardised model outputs.

3.3 Distribution of Microplastics in Habitats and Coral Compartments

3.3.1 Spatial comparison of MPs in corals and habitat sediments

Microplastics were detected across all sample types, with site-specific differences in concentration. In sediment samples, MPs were found at a mean concentration of 0.08 items cm^{-3}, ranging from 0.04 to 0.11 items cm^{-3} (Fig. 3.17 A). The highest concentrations were recorded at Double Island, followed by Crooked Island. In tissue samples, MPs were present at a mean concentration of 0.76 items cm^{-2}, with a range of 0.16 to 1.52 items cm^{-2} (Fig. 3.17 B). The highest concentration occurred at Crooked Island. MPs were also detected in coral skeletons at a mean concentration of 1.22 items cm^{-3}, ranging from 0.29 to 1.63 items cm^{-3} (Fig. 3.17 C). The highest values were observed at Port Island, followed by Crooked Island (1.52 items cm^{-3}) and Double Island (1.44 items cm^{-3}).

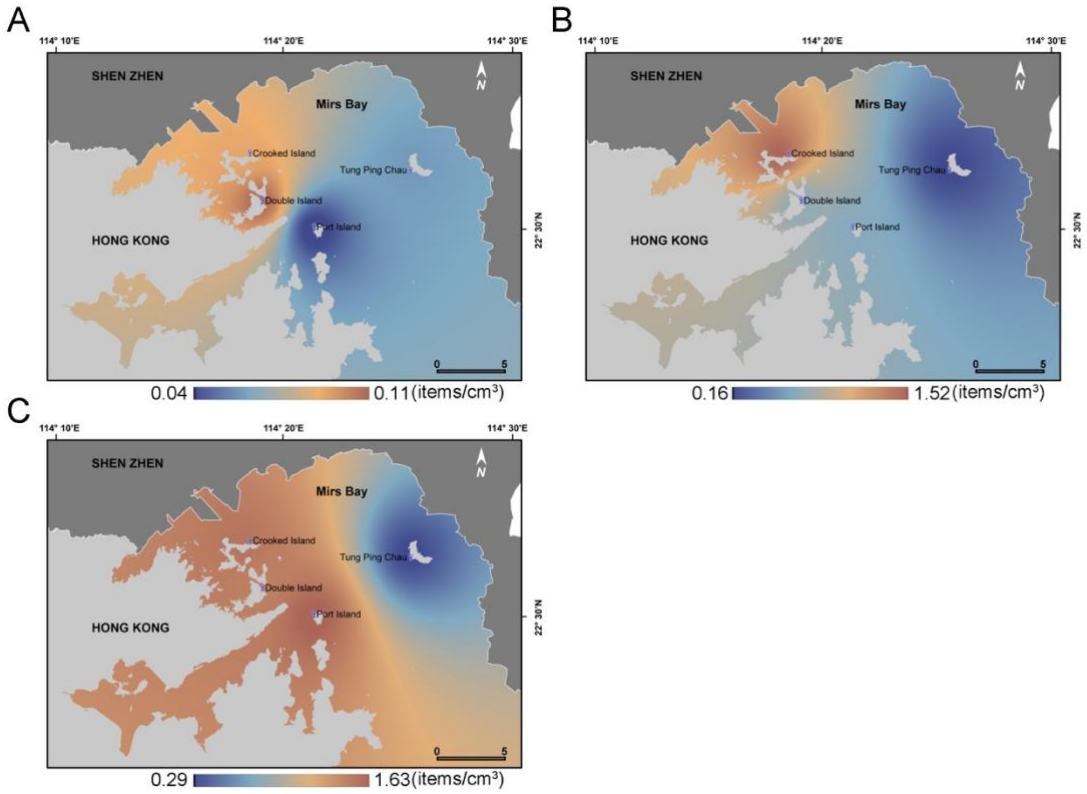

Figure 3. 17 QGIS maps of Mirs Bay showing the spatial distribution of MP concentrations in (A) sediments, (B) coral tissue, and (C) skeletons across four *P. acuta* habitats. Warmer colours (orange) indicate higher concentrations, while cooler colours (blue) represent lower concentrations.

3.3.2 Characteristics of MPs

The size distribution of MPs revealed a predominance of smaller particles across all sample types (Fig. 3.18 A). In sediment, coral tissue, and skeleton samples, the smallest size class (30-100 μm) was the most abundant, accounting for 43.1%, 53.1%, and 57.9%, respectively. This was followed by the 100-200 μm class (33.9%, 33.9%, and 30.3%), the 200-1000 μm class (21.3%, 12.7%, and 11.4%), and the largest size class (1000-5000 μm), which contributed less than 2.0% in all samples. Overall, the particle sizes of identified MPs ranged from 40 μm to 3233 μm.

Multiple polymer types were identified in the samples. PE, PET, PP, PS, and PMMA were present in all three sample types, while Nylon, PTFE, and PVC were detected exclusively in skeletons (Fig. 3.18 B). In sediments, PE, PET, PP, and PS were relatively evenly distributed at 14.6%, 23.4%, 25.6%, and 36.2%, respectively, with PMMA present at only 0.3%. PE and PP dominated in coral tissues (29.4% and 43.3%) and skeletons (51.8% and 25.2%), followed by PS and PET in both tissues (10.3% and 7.64%) and skeletons (14.2% and 7.45%). Nylon, PTFE, and PVC were detected in very low proportions in skeletons (0.3%, 0.1%, and 0.1%, respectively). Notably, PMMA accounted for 50% of MPs in coral tissue samples from Tung Ping Chau, a proportion significantly higher than at other sites. The highest polymer diversity was observed in coral skeletons (eight types), followed by tissue and sediment samples (five types each).

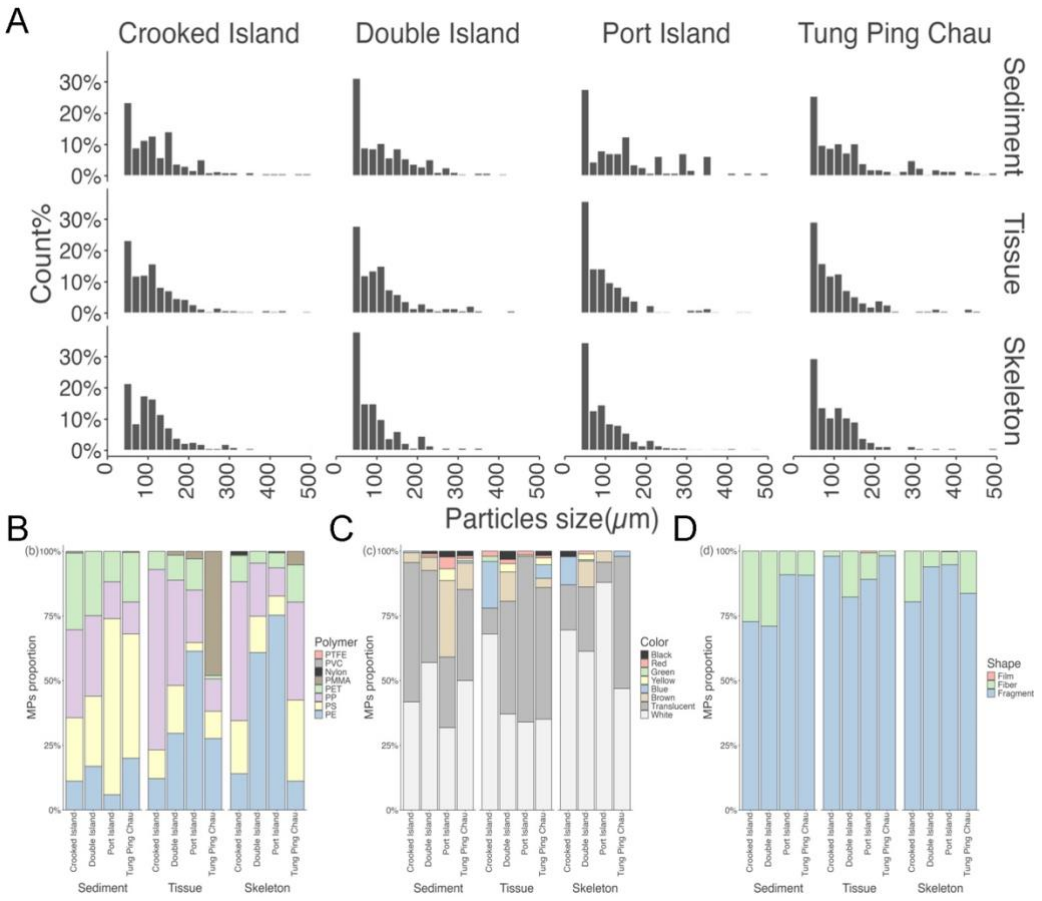

Figure 3. 18 Distribution and characteristics of MPs (MPs) across sampling sites. (A) Percentage of MPs by size class; (B) Percentage of polymer types; (C) Percentage of colours; (D) Percentage of particle shapes.

MPs exhibited a wide range of colours, including black, blue, brown, green, red, translucent, white, and yellow (Fig. 3.18 C). Translucent and white particles were dominant across all sample types: 40.4% and 48.6% in sediments, 49.3% and 39.4% in coral tissue, and 16.2% and 76.6% in skeletons. Brown and blue particles were the next most common, accounting for 3.2-7.8% and 0.4-4.0%, respectively. Other colours such as black, green, and yellow were present in minor amounts (≤1.3%). All polymers appeared predominantly as fragments, except PET, which occurred mostly as fibres.

In terms of morphology, MPs were primarily observed as fragments and fibres, with fragments being dominant across all sample types (Fig. 3.18 D). Fragments constituted 71-98% of all MPs particles, while fibres accounted for 2-29%. A small proportion of films (<0.6%) was found in tissue and skeleton samples, whereas no pellets were detected. These findings indicate that fragments are the dominant shape of MPs associated with corals and their habitats.

Morphological patterns also varied among polymer types: fragments were the predominant form for most polymers, including PE, PET, PS, PP, PMMA, Nylon, PTFE, and PVC. However, PET was most frequently observed in the form of fibres (88.6%).

3.3.3 Comparison of total MPs concentrations in coral skeletons and habitat sediments

Skeleton samples showed higher MPs concentrations than sediments across all sites, with the highest levels observed at Port Island (Fig. 3.19 A). The Bayesian zero-inflated beta model revealed significant sample-specific differences in total MPs concentrations (Fig. 3.19 B). Coral skeletons exhibited higher concentrations than sediments (skeleton = 2.23, 95% CI [1.00, 3.18]). No individual site (DI, PI, or TPC) showed a statistically credible baseline difference from the reference site (CI), as all site-level coefficients overlapped zero. The zero-inflation parameter was minimal (zi = 0.02, 95% CI [0.00, 0.09]), indicating negligible influence.

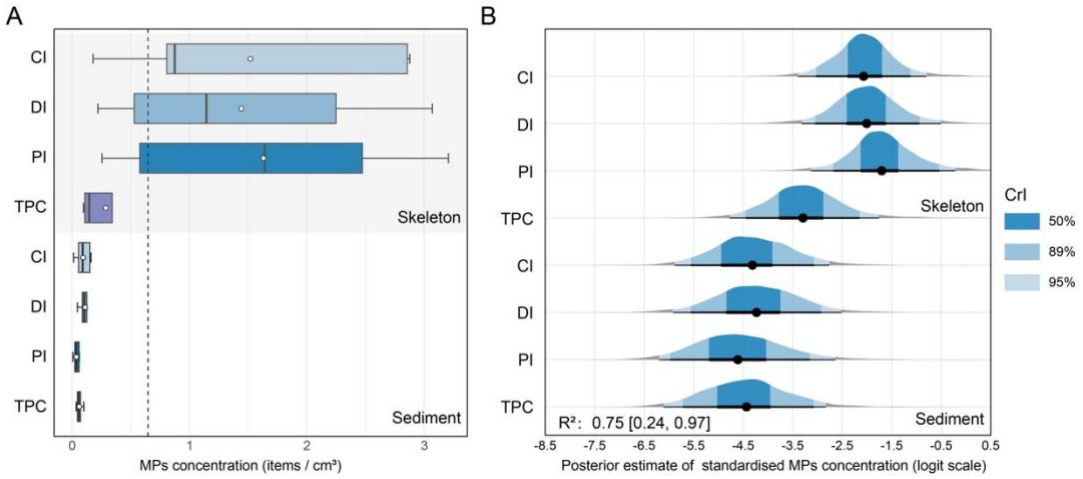

Figure 3. 19 Observed and modelled total MPs concentrations across sites and tissue types. (A) Boxplots show observed MPs concentrations (items cm^{-3}). Dots = means, lines = medians, boxes = IQR, whiskers = data spread. (B) Bayesian GLMM posterior distributions and CI of standardized total MPs concentrations. Dots = medians, and lines = 50%, 89% & 95% CI. Posterior R^2 values indicate model explanatory power.

Microplastic concentrations were higher in coral skeletons than in sediments across all sites, supported by strong evidence (95% CI) from Bayesian pairwise comparisons (Fig. 3.20). Sites comparisons within skeleton or sediment samples showed no credible differences, except for a

higher concentration in skeletons at Port Island compared to Tung Ping Chau with CI (89%) excluding zero. No differences were detected between sites in the sediment samples.

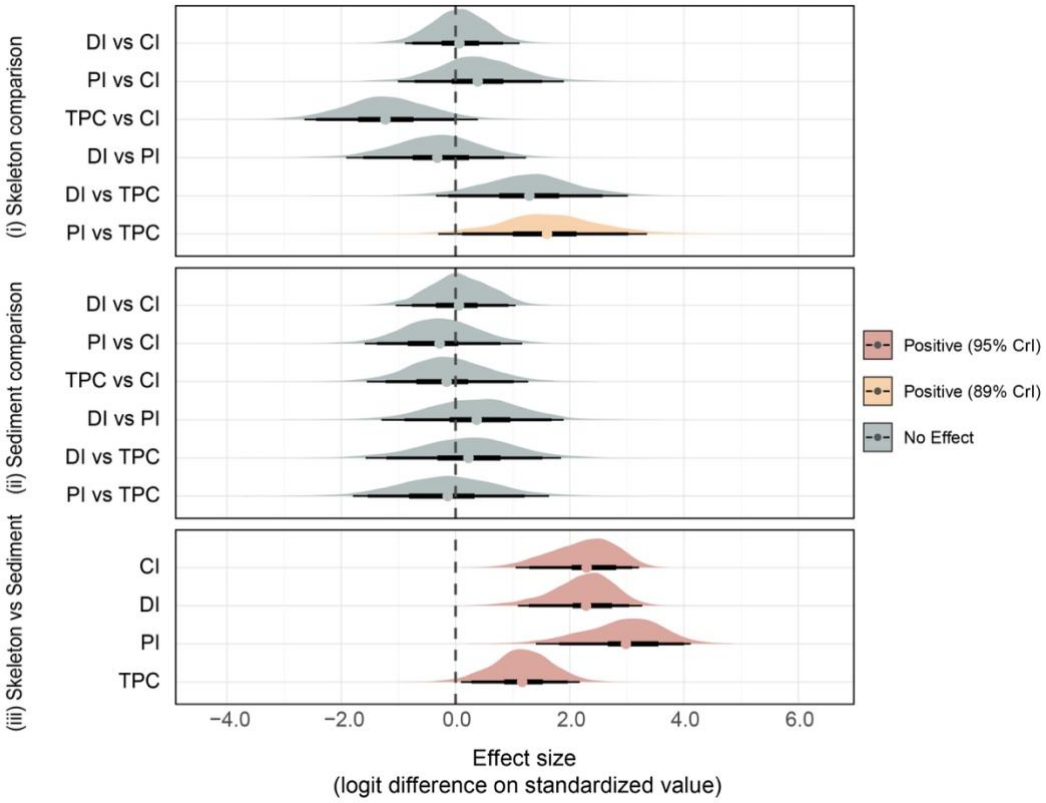

Figure 3. 20 Posterior estimates and hypothesis testing of standardised MPs concentrations across sites and tissue types. Density plots represent the effect size between pairs: i) sites within coral skeletons, ii) sites within sediments, iii) skeletons vs sediments within same site. Lines = 50%, 89% & 95%CI. Colours (blue=negative, red=positive, grey=non-significant) indicate statistical support. Estimates are based on standardised model outputs.

3.3.4 Comparison of polymer type composition (PE, PET, PS, PP) in coral skeletons and habitat sediments

The concentrations of PE, PET, PP, and PS varied across sites and sample types (Fig. 3.21). In coral skeletons, the highest PE concentration was observed at Port Island (1.30 items cm^{-3}), followed by Double Island (0.91 items cm^{-3}) and Crooked Island (0.22 items cm^{-3}). PET concentrations in skeletons ranged from 0.05 to 0.15 items cm^{-3}, with the highest value at Crooked Island. PP concentrations were 0.82 items cm^{-3} at Crooked Island and 0.29 items cm^{-3} at Double Island. PS concentrations ranged from 0.10 to 0.31 items cm^{-3}, with the highest at Crooked Island. In sediments, concentrations of all four polymers were lower. PE

concentrations ranged from 0.002 to 0.019 items cm^{-3}; PET ranged from 0.004 to 0.028; PP ranged from 0.005 to 0.035; and PS ranged from 0.023 to 0.031 items cm^{-3} across sites.

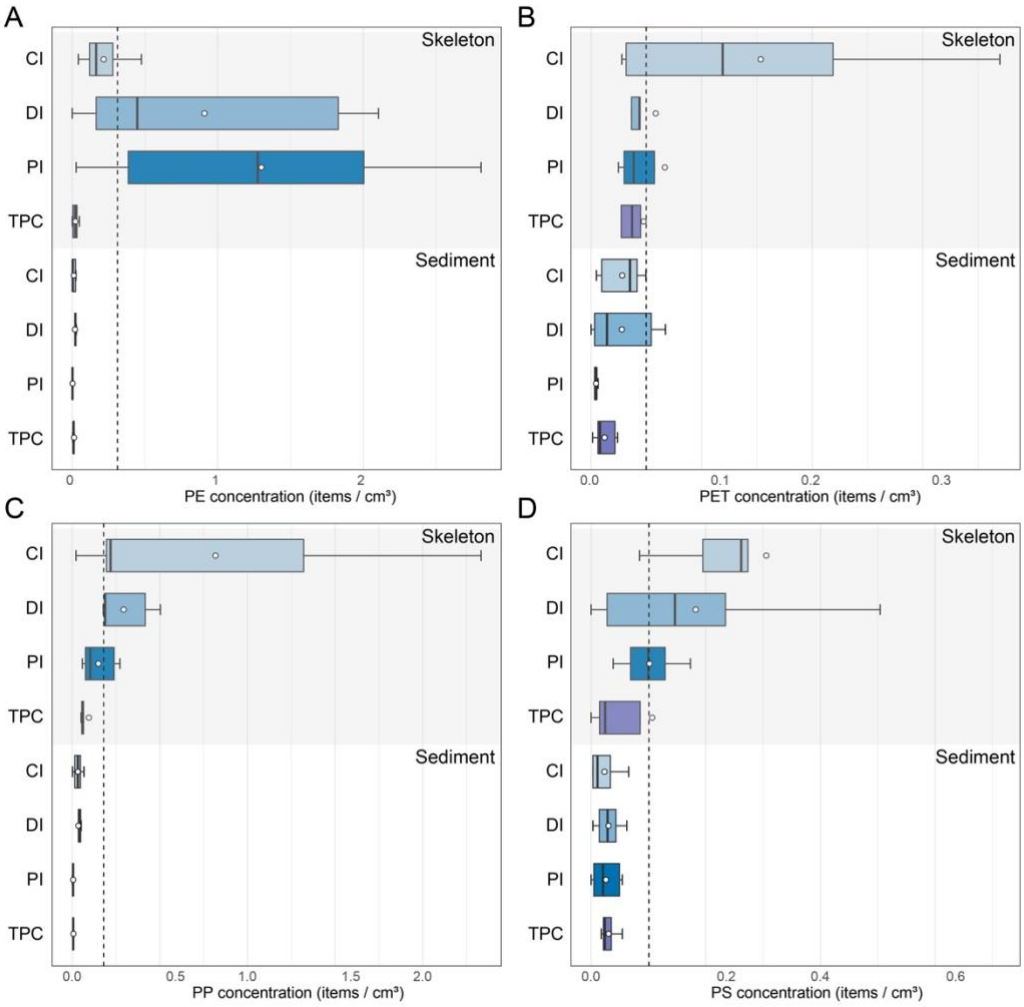

Figure 3. 21 Polymer-specific MPs concentrations in coral skeletons and habitat sediments. Boxplots show concentrations of PE (A), PET (B), PP (C), and PS (D) across sites (CI, DI, PI, and TPC). Dots = means, boxes = IQR, lines = medians, whiskers = data spread. Coral skeletons are shown in the upper shaded panels and sediments in the lower panels.

The Bayesian GLMM revealed PE showing the highest spatial and sample-specific accumulation. PE concentrations were consistently higher in coral skeletons compared to sediments across sites (posterior median log-odds, % [credible interval]: 2.28, 95% CI [1.46, 3.03]) (Fig. 3.22 A). These differences were modulated by sites. The positive interactions at Double Island (1.36, 95% CI [0.52, 2.20]) and Port Island (1.87, 95% CI [0.91, 2.80]) indicated greater skeletal PE accumulation in more urban-proximate areas. In contrast, a negative interaction at Tung Ping Chau (-1.43, 95% CI [-2.53, -0.28]) suggested relatively lower PE

concentrations in skeletons than sediments at this rural site. Main effects of site alone were not supported, indicating that type × site interactions primarily explained spatial variation. Other polymers showed consistent sample-specific effects without pronounced site-specific interactions. For PET (Fig. 3.22 B), skeletal concentrations were higher than sediments (1.09, 95% CI [0.31, 1.85]) without interaction of sites. Similar patterns were observed for PP and PS, where skeletons exhibited greater concentrations overall (PP: 1.35, 95% CI [0.46, 2.50]; PS: 1.83, 95% CI [1.03, 2.50]), but interactions with site were not meaningful. Model performance, indicated by R^2 values, further highlighted the significance of PE. The PE model was high in explanatory power (R^2 = 0.88, 95% CI [0.70, 0.98]) while the PS model showed moderate fit (R^2 = 0.63, 95% CI [0.20, 0.89]), and PET and PP models exhibited lower R^2 values (PET: R^2 = 0.30, 95% CI [0.08, 0.72]; PP: R^2 = 0.17, 95% CI [0.04, 0.63]).

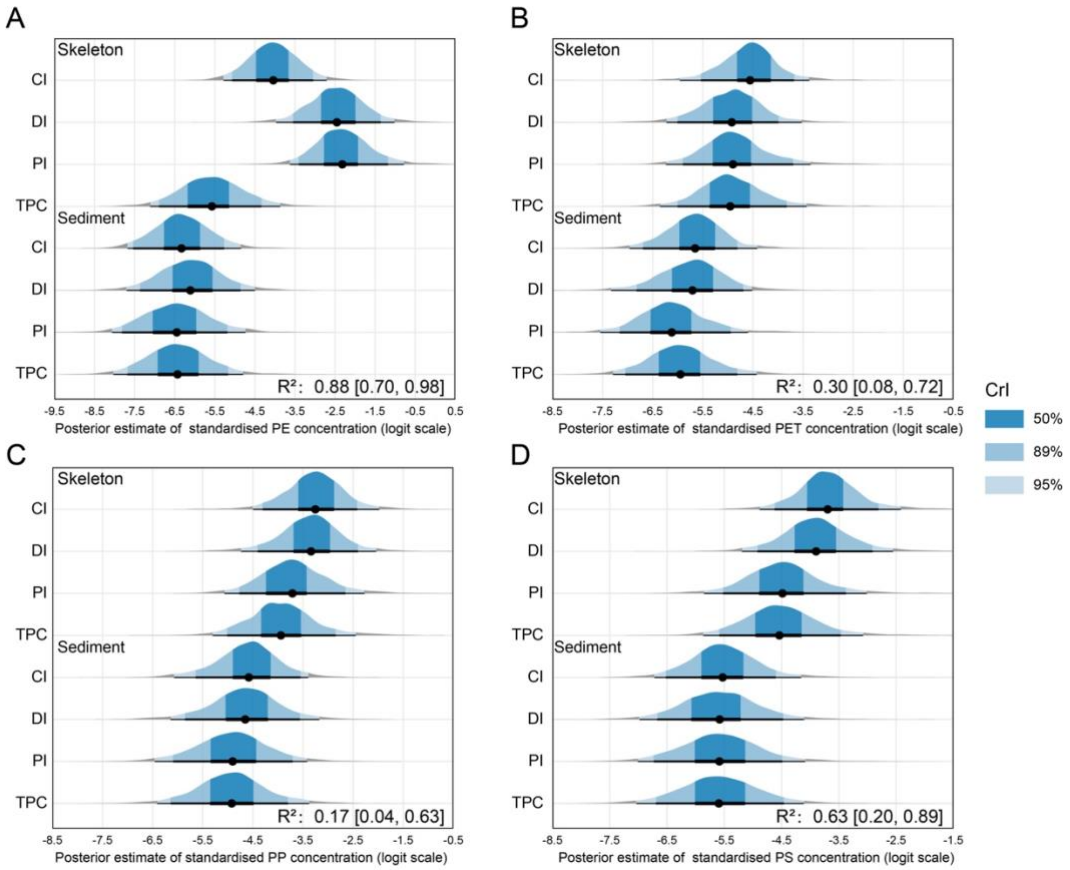

Figure 3. 22 Bayesian GLMM posterior distributions and CI of polymer-specific MPs concentrations in coral skeletons and habitat sediments. Standardised logit-scale concentrations of PE (A), PET (B), PP (C), and PS (D) are shown across sites (CI, DI, PI, and TPC). Dots = medians, and lines = 50%, 89% % 95% CI. Posterior R^2 values indicate model explanatory power. Coral skeletons are shown in the upper shaded panels and sediments in the lower panels.

The posterior estimates showed that coral skeletons were higher concentrations in four polymer types compared to sediments across sites (Fig. 3.23). For skeletal PE, additional differences were observed among sites, with Port Island and Double Island showing higher concentrations than Crooked Island, and Tung Ping Chau showing lower levels. No site-specific differences were evident for PET, PP, or PS within either sample type.

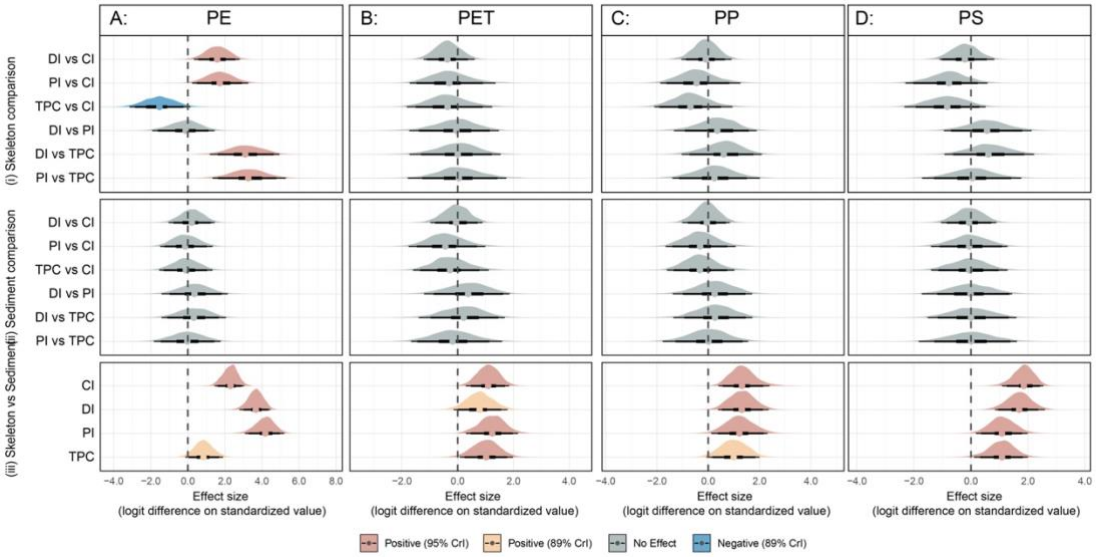

Figure 3. 23 Posterior estimates and hypothesis testing of polymer-specific MPs concentrations in coral skeletons and habitat sediments. Standardised logit-scale concentrations of PE (A), PET (B), PP (C), and PS (D) are shown across sites (CI, DI, PI, and TPC). Density plots represent the effect size between pairs: i) sites within coral skeletons, ii) sites within sediments, iii) skeletons vs sediments within same site. Lines = 50%, 89% & 95% CI; colours (blue = negative, red = positive, grey = non-significant) indicate statistical support. Estimates are based on standardised model outputs.

3.3.5 Microplastics distribution in corals

To account for differences in physical dimensions, MPs counts in tissues and skeletons were standardised by their respective mean reference areas/volumes (160.4 cm^2 for tissue, 115.8 cm^3 for skeleton) (Fig. 3.24). Across all sites, coral skeletons contained more MPs than tissues. On average, skeletons accounted for 71% of the total MPs found in coral samples. Nonetheless, tissue still contributed a substantial proportion of MPs, comprising 47.7% and 38.0% of the total MPs load in specimens from Tung Ping Chau and Crooked Island, respectively.

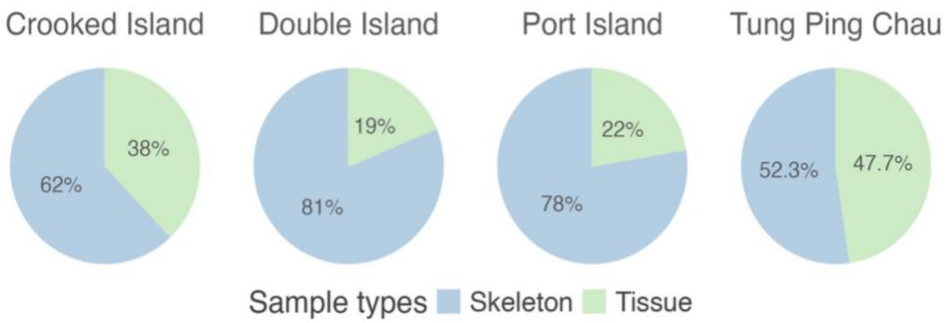

Figure 3. 24 Comparison of MPs distribution in coral tissues and skeletons, standardised by tissue area (160.4 cm^2) and skeleton volume (115.8 cm^3), respectively.

Chapter 4 – Discussion

4.1 Impacts of Microplastics on Coral Larvae

4.1.1 Influence of substrate conditioning and microplastics on larval settlement

The results indicate that substrate conditioning and microplastic (MP) exposure interact in complex, context-dependent ways to influence larval settlement. Consistent with prior studies (Negri & Hoogenboom, 2011; Perez et al., 2014; Webster et al., 2004), biologically conditioned tiles—enriched with microbial films and biochemical cues—promoted significantly higher settlement of *Acropora tumida* larvae compared to unconditioned tiles. Such conditioning mimics natural reef substrates by providing critical metamorphic signals from bacterial communities and crustose coralline algae (Jorissen et al., 2021; Tebben et al., 2015).

When examining the effects of zooxanthellae (Zx) and 10 μm polystyrene (PS) MPs, both separately and in combination (Mix), a nuanced pattern emerged. The Mix treatment reduced the settlement by approximately 38% (95% CI) on conditioned tiles whereas neither Zx nor PS alone produced a measurable effect. This pattern reflects an antagonistic interaction**.** One possible explanation is that PS may alter the role of ambient zooxanthellae, shifting them from facilitators to inhibitors of larval attachment. Liang et al. (2025) demonstrates that PS particles can induce oxidative stress in symbionts, increase extracellular polysaccharides production and alter the growth of associated bacteria. These findings suggest that the effect of zooxanthellae and PS particles may be mediated by multiple interacting mechanisms on coral settlement process. In present study, settlement was enhanced on conditioned tiles but this effect was partially compromised in mixed treatment. This inhibitory effect occurred only on biologically conditioned substrates suggests that PS-altered symbionts may specifically weaken positive settlement signals.

On unconditioned tiles, the settlement rates were significantly suppressed (95% CI) across all treatments, with settlement significantly lower compared with conditioned tiles. Exposure to zooxanthellae alone increased larval settlement from two percent in the control to seven percent, an absolute increase of approximately five percentage points. However, this increase was insufficient to compensate for the strong positive effect of natural microbial cues, which increased settlement by 17–33 percentage points on conditioned surfaces. Consistent with these

findings, Vermeij et al. (2013) reported that surfaces with attached zooxanthellae can enhance settler density up to 3.7-fold compared to surfaces without them. Other studies indicate that acquisition of *Symbiodinium* may shift larval substrate preference under stressed conditions (Winkler et al., 2015). Together, these findings suggest that zooxanthellae may act as an auxiliary settlement cue in environments lacking microbial biofilms, although their effect is relatively weak compared with biofilm-derived cues.

In contrast, PS alone exerted no significant effect on settlement or post-settlement growth, regardless of substrate conditioning. Ingestion of PS was infrequent (<5%), implying minimal physiological interaction or uptake. This neutral outcome aligns with findings by Berry et al. (2019); Liang et al. (2025), who observed limited toxicity from PS at lower concentrations (~10 mg/L).

Collectively, these findings highlight the need to assess multi-stressor interactions in coral settlement research. Components that appear beneficial in isolation (e.g., Zx) can become disruptive when combined with MPs under conditions that closely approximate natural reefs, potentially suppressing coral larval settlement in unexpected ways.

4.1.2 Limited impact of microplastics on larval growth and ingestion of microplastics

The experiment revealed that post-settlement growth was not significantly affected by any treatment, regardless of substrate conditioning or MP exposure. Bayesian generalized linear mixed model (GLMM) analysis confirmed that neither the experimental treatments nor tile conditioning had a measurable impact on the larvae's growth rates. Variance decomposition indicated that most variance was attributable to random factors (Tanks). It implied that larval growth is largely driven by variability of tank conditions rather than treatment effects. This result is consistent with Berry et al. (2019) who reports that microplastic contamination had limited effects on coral fertilization and early larval development. The direct impact of MPs on coral larvae may be less detrimental. Similarly, Kaposi et al. (2014) found restricted effects on marine larvae exposed to MPs under controlled conditions. However, Axworthy and Padilla-Gamino (2019) observed that chronic MP exposure can lead to species-specific stress responses, such as decreased coral growth. These contrasting findings emphasize resilience in

Acropora spp. but susceptibility to MPs may vary with species, exposure duration, and environmental context.

Besides, the ingestion rate of 10 μm polystyrene (PS) particles by larvae was found low (<1%). There is also no evidence of retention or physiological impairment. This low ingestion rate suggests that microplastic ingestion is a rare and transient event with limited potential for accumulation. Hankins et al. (2018) similarly found that scleractinian corals can egest most of ingested plastic particles. This finding reduces the likelihood of digestive blockages or chronic retention. Rotjan et al. (2019) also found selective ingestion and subsequent egestion in the temperate coral *Astrangia poculata*. To conclude, ingestion does not necessarily translate to long-term accumulation or harm.

However, contrasting findings exist. Zhou et al. (2023) reported that some coral species, such as *Porites pukoensis*, can accumulate MPs, leading to physiological disruptions. The absence of accumulation in this study suggests that susceptibility to MP retention may be species-specific. Although Bove et al. (2023) found that MP exposure may trigger immune responses in the absence of growth or behavioral changes, it seems the effect of microplastics can be influenced by factors such as feeding mode, particle size, or developmental stage. This interpretation is supported by Berry et al. (2019), who observed limited MP effects on coral fertilization and larval development. It seems coral larvae is somehow resilient during early life stages. McCormick et al. (2020) further emphasized that MP ingestion alone may not alter behavior or survival unless compounded by other stressors or environmental degradation.

Collectively, these findings provide more insights into coral larval interactions with microplastics. Although ingestion of small particles does occur, there is no evidence of accumulation or adverse effects on early development. Future research should aim to clarify under which conditions MP ingestion might progress to accumulation.

4.2 Impacts of Microplastics on Juvenile and Adult Corals

4.2.1 Life-stage dependent Sensitivity to microplastics

The experimental findings demonstrate a clear life-stage-dependent sensitivity to microplastics (MPs) in *A. tumida*. Juvenile corals exhibit pronounced vulnerability to polypropylene (PP) exposure. In juvenile *A. tumida*, exposure to PP significantly impairs essential growth metrics. Surface area expansion decreases to 117.7% in PP treatments compared to 139.2% in controls and polyp counts decline further relative to controls. Photochemical efficiency is similarly compromised, as indicated by notable increases in gray scale values and reductions in Fo. In contrast, exposure to PET shows no credible impact on growth or photochemical parameters, while sediment treatment does not affect these metrics either—except that it significantly reduces polyp numbers. However, those mentioned adverse effects were not seen in the experiments of adult corals.

Adult *A. tumida* are resilient under all treatment conditions. Measurements of buoyant weight remained stable across all treatments, with Bayesian models indicating negligible impact (R^2 = 0.99 and credible intervals overlapping zero). Photochemical parameters in adult colonies similarly showed no credible changes, with wide credible intervals and high percentages indicating little to no effect. This resilience is consistent with previous studies; for example, Grillo et al. (2021) reported short-term resilience in adult *Porites* against microplastic exposure, as evidenced by the absence of mortality or activation of stress biomarkers following polystyrene ingestion. Such resilience in adults may be attributed to physiological adaptations, such as enhanced heterotrophic capacity and energy reserves, as demonstrated by corals in turbid environments (Anthony, 2000). Goodkin et al. (2011) revealed that Hong Kong corals not only thrive under high turbidity but also endure large fluctuations in salinity and temperature—conditions that most tropical reef corals typically cannot tolerate. In comparison, studies on tropical adult corals have reported adverse effects, for example, bleaching and tissue necrosis (Hierl et al., 2021; Reichert et al., 2018). The apparent tolerance toward microplastics may result from an adaptive response by corals to these variable environmental conditions.

The heightened sensitivity observed in juveniles may result from developmental limitations. Early life stages are typically characterized by underdeveloped protective mechanisms, including less robust mucus production and immature associations with symbiotic algae, which

render them more vulnerable to environmental stressors. Across multiple studies, juvenile corals are consistently shown to be more sensitive to environmental stressors than adults. This heightened sensitivity is reflected in higher mortality rates under pollution and disturbance (McKenna et al., 2001; Tietjen et al., 2025), challenges in establishing symbiosis (Yuyama et al., 2018), and limited capacity to sustain energetically costly stress responses such as mucus production (Bessell-Browne et al., 2017; Brown & Bythell, 2005). Therefore, the immaturity and unstable of symbiosis of juveniles results in limited energy reserve and ability to stress induced by microplastics. Additionally, juveniles have a higher surface-to-volume ratio, potentially increasing interactions with suspended MPs and thereby exacerbating physiological stress. This study also noted a reduction in polyp counts under PP exposure, suggesting either physical disruption of polyp budding or compromised tissue integrity. Similar reductions in polyp numbers have been reported under other stressors, such as competition with macroalgae (Webster et al., 2015), indicating that polyp suppression may be a generalizable response to environmental challenges. The reduce surface area and polyp number highlight the vulnerability of juvenile corals at both structural and functional levels.

Despite the observed short-term resilience in adult corals, it is important to recognize that chronic MP exposure could pose latent risks over longer timescales. Prolonged exposure may result in the gradual depletion of energy reserves, diminished reproductive success, or increased vulnerability to secondary stressors such as pathogenic infections or thermal anomalies. Therefore, while the protection of juvenile corals is critical for reef recruitment and future resilience, comprehensive long-term studies on adult impacts remain necessary to fully assess the ecological consequences of persistent MP exposure.

4.2.2 Different toxicity of microplastic polymers

The results reveal significant polymer-specific differences in the toxicity of microplastics to *A. tumida*. Juvenile corals exposed to PP exhibit clear signs of stress compared to those exposed to PET or sediments. PP exposure results in a notable increase in grey scale values and a reduction in Fo, accompanied by non-significant declines in Fv/Fm and Abs. These changes suggest early bleaching events, possibly due to partial loss of symbionts or degradation of pigments. In contrast, exposure to PET produces no significant changes in growth or photochemical responses, and sediment treatments leave these parameters largely unaffected—

except for a marked reduction in polyp numbers. Overall, PP is evidently more toxic than both PET and sediment, and these findings are consistently supported by Bayesian statistical models.

These results align with existing research on microplastic toxicity in marine systems. For example, Chen et al. (2022) reported oxidative stress and tissue damage in juvenile *Goniopora columna* exposed to polyethylene (PE), a polymer sharing PP's buoyant and hydrophobic properties. Corinaldesi et al. (2021) showed that PP caused the most severe effects—reduced feeding, excess mucus production, tissue damage, microbial shifts, and elevated stress gene expression—among the five tested polymers (PP, PE, PS, PET, and PVC), likely due to its buoyancy and biofilm-coated surface mimicking food cues that led to higher ingestion by corals. In addition, the different densities of PP, PET and sediment influence their suspension in vertically mixed water and thus coral accessibility. PP, with low and uniform density, likely stays suspended and causes the most severe effects; sediment, with variable density and shapes, may be partially resuspended and has moderate effects; and dense PET, with narrow high-density range, sinks quickly, resulting in minimal impact.

The minimal effect of PET and sediment align to the result of Ng and Todd (2023), which also highlight the PET, with lower density than sediment, may pose less shear force on corals. The sinking property and relative low density of PET result in lower exposure and shearing force on coral. Corals in Hong Kong survived under turbid water are adapted to heavier load of settling particles. Apart from growth, photosynthesis is normal under PET treatment and another study shows coral is capable to maintain normal photosynthesis under 10x higher concentration of PET particles than 10 mg/L, used in present study. Therefore, PET may pose lower physical disruption than PP and sediment. For sediment, polyp count reduction is recorded without reduced tissue expansion or sign of bleaching. Polyp formation is a process after tissue expansion (Lin et al., 2022). Normal tissue expansion but budding suppression indicate a slower growth of juvenile in sediment treatment. PP treatment, however, suppress both tissue expansion and polyp formation. Low density of PP particles encourages the resuspension and thus repeated exposure, which increases the energy expense during clearance processes, although coral found to capable to ingest and egest microplastics.

Apart from inhibiting growth, bleaching was also evident, as demonstrated by increased grey scale values coupled with a decline in Fo. The reduction in Fo indicates lowered total

fluorescence, which may result from a diminished density of symbionts. Similar bleaching responses have been observed following exposure to other polymers such as PVC (Rotjan et al., 2019), PE (Syakti et al., 2019), and PS (Su et al., 2020). These effects may arise either from a direct disruption of coral physiology or indirectly through a reduction in photosynthesis caused by shading from microplastics. Moreover, some studies have observed an increased Fv/Fm value as a short-term compensatory response to shading (Reichert et al., 2019; Rocha et al., 2020); however, this study recorded a reduced Fv/Fm value. This discrepancy may be explained by the low-light tolerance of the experimental species, *A. tumida*, which is adapted to the turbid waters of Hong Kong (Yeung et al., 2021). Additionally, several *Acropora* species have been observed to shift towards a more heterotrophic mode under turbid conditions (Travaglione et al., 2023; Zweifler et al., 2024), suggesting that rather than enhancing photosynthetic efficiency, heterotrophy may be the primary strategy by which *A. tumida* survives in both experimental and native environments.

4.3 Distribution of Microplastics in Corals and Habitats in Mirs Bay

4.3.1 Coral skeletons as a long-term Sink

The findings obtained in this study reinforce that stony corals are not merely transient traps for microplastics (MPs) but may serve as long-term living sinks. Recent research has suggested that coral skeletons serve as biological “time capsules” for MPs (Corona et al., 2020; Reichert et al., 2022). In current work, coral skeletons contained approximately 10 to 15-fold more MPs (per unit volume) than surrounding sediments. The posterior estimates consistently showed significant accumulation by polymers PE, PET, PP and PS. In addition, the lower zero inflation in skeletons relative to sediments (see Fig. 3.19 B) indicates the significant accumulation in skeletons. This supports the idea that coral skeletons may serve as long-term archives, preserving a cumulative record of MP exposure. Such accumulation in corals likely arises from multiple processes. One possibility is heterotrophic ingestion, whereby coral polyps capture MP particles and subsequently translocate them from tissue into the skeleton via ingestion processes (Hall et al., 2015; Reichert et al., 2018). Alternatively, MPs that settle onto the coral coenosarcs may become passively entrapped by overgrowth and subsequently sealed into the aragonite matrix.

In addition to comparisons with adjacent sediments, internal contrasts between coral compartments provide further insight into the retention mechanisms. On average, the coral skeleton archived approximately 71% of the total MPs affirming its dominant role in long-term sequestration. However, the tissue compartment accounted for a considerable proportion of the total MP load in specific locations (e.g., 47.7% at Tung Ping Chau and 38.0% at Crooked Island), potentially reflecting spatial heterogeneity in environmental exposure or variability in local environment (Lo et al., 2018; Tsang et al., 2017). Despite these variations, the broader pattern remains that most MPs are ultimately archived in the skeletal matrix.

The protective aragonite structure of coral skeletons provides an environment that minimizes the risk of resuspension and degradation, ensuring that embedded MPs remain immobilized over extended timeframes (Raguso et al., 2022; Reichert et al., 2022). By capturing both the quantity and polymer diversity of microplastics, the coral skeleton offers a temporally integrated signal of MP exposure, which is of considerable value for marine pollution monitoring (Corona et al., 2020; Tang et al., 2021). The findings support the view that coral skeletons represent the primary biogenic sink for microplastics within reef systems, providing a critical archive of historical and ongoing plastic contamination.

4.3.2 Spatial and sample-type patterns in polymer composition

Spatial patterns in skeletal polyethylene (PE) concentrations varied significantly among sites within Mirs Bay, as supported by Bayesian generalized linear mixed models (GLMMs). Coral skeletons at Port Island and Double Island exhibited statistically higher PE loads relative to the Tung Ping Chau Marine Park. Meanwhile, Crooked Island showed elevated microplastics concentrations but did not differ significantly from all other sites. Port Island, Double Island and Crooked Island are on the West of the bay and proximate to the mouth of Tolo Harbour and adjacent to Yantian International Container Terminal, which are potentially sources of urban pollution. Tung ping Chau, however, locate in a marine park at the eastern margin of the Bay, where is more rural and sparsely populated. It seems the sites near the urban area are positively associated with increasing microplastic concentration in the bay. These results are in line with previous investigations that proximity to anthropogenic sources was linked to elevated microplastic loads in biogenic structures (Reichert et al., 2022; Tsang et al., 2017).

Coral skeletons accumulated higher amount of microplastics, especially PE, but it may not represent the environmental concentration. The MPs concentration did not differ significantly across sites in sediment, which is considered as a proxy for ambient concentration in several studies (Cheang et al., 2018; Lo et al., 2018; Tsang et al., 2017). Bayesian analysis revealed no credible site-level differences in sediment PE concentrations, with all credible intervals overlapping zero. It implied that PE at the seabed level was relatively uniform throughout Mirs Bay. Similar conclusions were drawn by Tsang et al. (2017), who reported spatial uniformity in sediment microplastic levels despite marked differences in nearby urban impacts.

Consequently, the spatial differences in skeletal PE accumulation are unlikely to be explained solely by variations in seabed exposure. Instead, these patterns likely reflect biologically mediated retention processes such as mucosal trapping, particle ingestion, and subsequent skeletal overgrowth, combined with variations in local exposure dynamics not captured by sediment sampling (Jandang et al., 2024; Reichert et al., 2022). The observed enrichment of PE in coral skeletons at urban-proximate sites may thus represent a combined outcome of cumulative exposure history and ecological filtering mechanisms. These findings align with the proposition by Reichert et al. (2022) that skeletal microplastics are likely the product of both biological and spatially influenced rather than as a direct indicator of ambient microplastic concentrations. Another study also report PE is found highest amount in coral among the other polymers Raguso et al. (2022). Although the study does not provide the ambient PE concentration, it still proves the enrichment of PE in corals.

In contrast, while polypropylene (PP) was also frequently detected in coral compartments, the statistical differentiation among tissue, skeleton, and sediment was not significant. While both polyethylene terephthalate (PET) and polystyrene (PS) showed proportionally higher concentrations in the skeletons relative to other compartments, these patterns lacked statistical robustness. Similar patterns are also reported in other studies (Cheang et al., 2018; Ding et al., 2019). Occasionally, a few particles identified as nylon, polytetrafluoroethylene (PTFE), or polyvinyl chloride (PVC) were detected in skeletal samples but lack of statistical significance. The presence of rare polymers might reflect occasional environmental exposure rather than consistent retention patterns.

Chapter 5 - Conclusion

5.1 Summary of Key Findings

This thesis set out to clarify the influence of microplastics (MPs) on hard corals across their life-history trajectory, addressing a gap in the literature in which most studies have treated life stages and exposure routes in isolation. Three principal questions were posed: (1) to what extent MPs affect larval settlement, post-settlement growth and the acquisition of *Symbiodinium*; (2) how polymer types affect the growth and photosynthesis of juvenile and adult colonies; and (3) whether reef-building corals act as long-term sink for MPs, and, if so, which polymers prevail in their skeletons relative to surrounding sediments.

To resolve these questions a multi-level experimental–field framework was adopted. In the laboratory, *Acropora tumida* larvae, juveniles and adults were exposed to different concentration and sources of microplastics, e.g. polystyrene (PS), polypropylene (PP) and polyethylene terephthalate (PET). Responses were evaluated with Bayesian generalised linear mixed-effects models (GLMMs), a statistical approach that yields probabilistic estimates robust to small and heterogeneous datasets. Field sampling in Mirs Bay quantified MPs in paired samples of *P. acuta* skeletons and adjacent sediments via Raman mapping and three-dimensional volumetric normalization.

Stage-specific sensitivities emerged. For larvae, conditioning of the settlement substrate explained most variation in settlement success, whereas PS combined with zooxanthellae suppressed settlement on conditioned tiles by 38 %, implying that PS-altered symbiont cues can override positive biofilm signals. PS ingestion was negligible, supporting observations that early coral stages can rapidly egest small plastic particles. Juveniles proved highly susceptible to PP: tissue expansion and polyp budding declined by 16–22 % and early photochemical indicators signaled bleaching, while PET and natural sediment elicited only subtle effects. Adults, in contrast, maintained buoyant weight and photosynthesis efficiency under all treatments, indicating short-term tolerance likely sustained by heterotrophic feeding and mucus-mediated clearance.

In field study, coral skeletons contained MP concentrations an order of magnitude higher than neighbouring sediments, with PE fragments (30–100 μm) dominant at urban-proximate sites, confirming skeletons as living archives of microplastic pollution (Reichert et al., 2022).

The study advances knowledge on several fronts. First, by integrating responses across life stages it refines ecological-risk assessments that have hitherto assumed uniform coral sensitivity. Second, the demonstration that PP is markedly more deleterious than PET provides polymer-specific evidence to inform source-reduction policies. Third, the coupling of Bayesian GLMMs with Raman mapping and three dimensions scanning offers a reproducible template for quantifying skeletal MPs and detecting subtle biological effects.

5.2 Limitations and Further Studies

Laboratory exposures were restricted to short period and thus cannot capture chronic consequences. However, the effect of microplastic already affect recruits with adverse effect in 30 days so it may suggest the higher vulnerability of recruit in wilds. Also, this work focused on three polymers within a limited size class (10–106 μm), whereas reefs experience a broader spectrum, including nano-scale particles and additive-laden debris. The result may not be solely applicable to realistic consequence but rather act as a reference and comparison with other studies to reveal some possible interaction effects between microplastics and corals.

Future studies should therefore: (1) implement long-term and multigenerational exposures to reveal trade-offs between growth and fecundity; (2) examine the toxicity of particles in other size range, e.g. nanoplastics, to elucidate mechanistic pathways of oxidative stress; (3) as coral skeletons are proven as a sink of microplastics, it help to develop skeletal chronology approaches to couple annual growth bands with polymer deposition and reconstruct historical MP trends.

In summary, the impact of MPs on corals is heterogeneous and context-dependent, varying with life stage, polymer identity and local environmental conditions. The findings refine theoretical understanding, inform targeted mitigation strategies and provide a methodological scaffold for future investigations aimed at safeguarding coral-reef resilience under escalating anthropogenic pressure.

References

Allen, A. S., Seymour, A. C., & Rittschof, D. (2017). Chemoreception drives plastic consumption in a hard coral. *Marine Pollution Bulletin*, *124*(1), 198-205.

Anthony, K. R. N. (2000). Enhanced particle-feeding capacity of corals on turbid reefs (Great Barrier Reef, Australia). *Coral Reefs*, *19*(1), 59-67.

Axworthy, J. B., & Padilla-Gamino, J. L. (2019). Microplastics ingestion and heterotrophy in thermally stressed corals. *Scientific Reports*, *9*(1), 18193.

Babcock, R., & Davies, P. (1991). Effects of sedimentation on settlement of *Acropora millepora*. *Coral Reefs*, *9*(4), 205-208.

Babcock, R., & Mundy, C. (1996). Coral recruitment: Consequences of settlement choice for early growth and survivorship in two scleractinians. *Journal of Experimental Marine Biology and Ecology*, *206*(1-2), 179-201.

Bashir, S. M., Kimiko, S., Mak, C.-W., Fang, J. K.-H., & Gonçalves, D. (2021). Personal Care and Cosmetic Products as a Potential Source of Environmental Contamination by Microplastics in a Densely Populated Asian City. *Frontiers in Marine Science*, *8*.

Berry, K. L. E., Epstein, H. E., Lewis, P. J., Hall, N. M., & Negri, A. P. (2019). Microplastic Contamination Has Limited Effects on Coral Fertilisation and Larvae. *Diversity*, *11*(12), 228.

Bessell-Browne, P., Negri, A. P., Fisher, R., Clode, P. L., Duckworth, A., & Jones, R. (2017). Impacts of turbidity on corals: The relative importance of light limitation and suspended sediments. *Marine Pollution Bulletin*, *117*(1-2), 161-170.

Bove, C. B., Greene, K., Sugierski, S., Kriefall, N. G., Huzar, A. K., Hughes, A. M., Sharp, K., Fogarty, N. D., & Davies, S. W. (2023). Exposure to global change and microplastics elicits an immune response in an endangered coral. *Frontiers in Marine Science*, *9*.

Brandon, J. A., Jones, W., & Ohman, M. D. (2019). Multidecadal increase in plastic particles in coastal ocean sediments. *Science Advances*, *5*(9), eaax0587.

Brandt, J., Bittrich, L., Fischer, F., Kanaki, E., Tagg, A., Lenz, R., Labrenz, M., Brandes, E., Fischer, D., & Eichhorn, K.-J. (2020). High-Throughput Analyses of Microplastic Samples Using Fourier Transform Infrared and Raman Spectrometry. *Applied Spectroscopy*, *74*(9), 1185-1197.

Brown, B. E., & Bythell, J. C. (2005). Perspectives on mucus secretion in reef corals. *Marine Ecology Progress Series*, *296*, 291-309.

Bürkner, P.-C. (2017). brms : An R Package for Bayesian Multilevel Models Using Stan. *Journal of Statistical Software*, *80*(1), 1-28.

Chandler, J. F., Figueira, W. F., Burn, D., Doll, P. C., Johandes, A., Piccaluga, A., & Pratchett, M. S. (2024). Predicting 3D and 2D surface area of corals from simple field measurements. *Scientific Reports*, *14*(1), 20549.

Cheang, C. C., Ma, Y., & Fok, L. (2018). Occurrence and Composition of Microplastics in the Seabed Sediments of the Coral Communities in Proximity of a Metropolitan Area. *International Journal of Environmental Research and Public Health*, *15*(10).

Chen, Y. T., Ding, D. S., Lim, Y. C., Singhania, R. R., Hsieh, S., Chen, C. W., Hsieh, S. L., & Dong, C. D. (2022). Impact of polyethylene microplastics on coral Goniopora columna causing oxidative stress and histopathology damages. *Science of the Total Environment*, *828*, 154234.

Cho, Y., Shim, W. J., Ha, S. Y., Han, G. M., Jang, M., & Hong, S. H. (2023). Microplastic emission characteristics of stormwater runoff in an urban area: Intra-event variability and influencing factors. *Science of the Total Environment*, *866*, 161318.

Chui, A. P. Y., & Ang, P. (2015). Elevated temperature enhances normal early embryonic development in the coral *Platygyra acuta* under low salinity conditions. *Coral Reefs*, *34*(2), 461-469.

Chui, A. P. Y., & Ang, P., Jr. (2017). High tolerance to temperature and salinity change should enable scleractinian coral *Platygyra acuta* from marginal environments to persist under future climate change. *PLoS One*, *12*(6), e0179423.

Chui, A. P. Y., Wong, M. C., Liu, S. H., Lee, G. W., Chan, S. W., Lau, P. L., Leung, S. M., & Ang, P. (2014). Gametogenesis, Embryogenesis, and Fertilization Ecology of " *Platygyra acuta* " in Marginal Nonreefal Coral Communities in Hong Kong. *Journal of Marine Biology*, *2014(2014)*, 1-9.

Cole, M., Webb, H., Lindeque, P. K., Fileman, E. S., Halsband, C., & Galloway, T. S. (2014). Isolation of microplastics in biota-rich seawater samples and marine organisms. *Scientific Reports*, *4*, 4528.

Corinaldesi, C., Canensi, S., Dell'Anno, A., Tangherlini, M., Di Capua, I., Varrella, S., Willis, T. J., Cerrano, C., & Danovaro, R. (2021). Multiple impacts of microplastics can threaten marine habitat-forming species. *Communications Biology*, *4*(1), 431.

Corona, E., Martin, C., Marasco, R., & Duarte, C. M. (2020). Passive and Active Removal of Marine Microplastics by a Mushroom Coral (*Danafungia scruposa*). *Frontiers in Marine Science*, *7*.

Cowles, M. K., & Carlin, B. P. (1996). Markov Chain Monte Carlo Convergence Diagnostics: A Comparative Review. *Journal of the American Statistical Association*, *91*, 883-904.

Ding, J., Jiang, F., Li, J., Wang, Z., Sun, C., Wang, Z., Fu, L., Ding, N. X., & He, C. (2019). Microplastics in the Coral Reef Systems from Xisha Islands of South China Sea. *Environmental Science & Technology*, *53*(14), 8036-8046.

Eriksen, M., Lebreton, L. C., Carson, H. S., Thiel, M., Moore, C. J., Borerro, J. C., Galgani, F., Ryan, P. G., & Reisser, J. (2014). Plastic Pollution in the World's Oceans: More than 5 Trillion Plastic Pieces Weighing over 250,000 Tons Afloat at Sea. *PLoS One*, *9*(12), e111913.

Falkowski, P. G., Dubinsky, Z., Muscatine, L., & McCloskey, L. (1993). Population control in symbiotic corals: ammonium ions and organic materials maintain the density of zooxanthellae. *Bioscience*, *43*(9), 606-611.

Fang, J. K. H., Schönberg, C. H. L., Kline, D. I., Hoegh-Guldberg, O., & Dove, S. (2013). Methods to quantify components of the excavating sponge Cliona orientalis Thiele, 1900. *Marine ecology*, *34*(2), 193-206.

Fang, J. K. H., Schönberg, C. H. L., Mello-Athayde, M. A., Achlatis, M., Hoegh-Guldberg, O., & Dove, S. (2018). Bleaching and mortality of a photosymbiotic bioeroding sponge under future carbon dioxide emission scenarios. *Oecologia*, *187*(1), 25-35.

Gaither, M. R., & Rowan, R. (2010). Zooxanthellar symbiosis in planula larvae of the coral *Pocillopora damicornis*. *Journal of Experimental Marine Biology and Ecology*, *386*(1-2), 45-53.

Goldstein, M. C., Rosenberg, M., & Cheng, L. (2012). Increased oceanic microplastic debris enhances oviposition in an endemic pelagic insect. *Biology Letters*, *8*(5), 817-820.

Goodkin, N. F., Switzer, A. D., McCorry, D., DeVantier, L., True, J. D., Hughen, K. A., Angeline, N., & Yang, T. T. (2011). Coral communities of Hong Kong: long-lived corals in a marginal reef environment. *Marine Ecology Progress Series*, *426*, 185-196.

Grillo, J. F., Sabino, M. A., & Ramos, R. (2021). Short-term ingestion and tissue incorporation of Polystyrene microplastic in the scleractinian coral *Porites porites*. *Regional studies in marine science*, *43*, 101697.

Hall, N. M., Berry, K. L. E., Rintoul, L., & Hoogenboom, M. O. (2015). Microplastic ingestion by scleractinian corals. *Marine Biology*, *162*(3), 725-732.

Hankins, C., Duffy, A., & Drisco, K. (2018). Scleractinian coral microplastic ingestion: Potential calcification effects, size limits, and retention. *Marine Pollution Bulletin*, *135*, 587-593.

Harii, S., Yamamoto, M., & Hoegh-Guldberg, O. (2010). relative contribution of dinoflagellate photosynthesis and stored lipids to the survivorship of symbiotic larvae of the reef-building corals. *Marine Biology*, *157*(6), 1215-1224.

Harii, S., Yasuda, N., Rodriguez-Lanetty, M., Irie, T., & Hidaka, M. (2009). Onset of symbiosis and distribution patterns of symbiotic dinoflagellates in the larvae of scleractinian corals. *Marine Biology*, *156*(6), 1203-1212.

Herler, J., & Dirnwober, M. (2011). A simple technique for measuring buoyant weight increment of entire, transplanted coral colonies in the field. *Journal of Experimental Marine Biology and Ecology*, *407*(2), 250-255.

Hierl, F., Wu, H. C., & Westphal, H. (2021). Scleractinian corals incorporate microplastic particles: identification from a laboratory study. *Environmental Science and Pollution Research International*, *28*(28), 37882-37893.

Ho, Y. W., Lim, J. Y., Yeoh, Y. K., Chiou, J. C., Zhu, Y., Lai, K. P., Li, L., Chan, P. K. S., & Fang, J. K. (2022). Preliminary Findings of the High Quantity of Microplastics in Faeces of Hong Kong Residents. *Toxics*, *10*(8).

Howlett, R. (1995). [Review of the book Life in Moving Fluids: The Physical Biology of Flow (2nd ed.), by S. Vogel]. *Nature*, *373*(6510), 114.

Huang, W., Chen, M., Song, B., Deng, J., Shen, M., Chen, Q., Zeng, G., & Liang, J. (2021). Microplastics in the coral reefs and their potential impacts on corals: A mini-review. *Science of the Total Environment*, *762*, 143112.

Huang, Z., Hu, B., & Wang, H. (2023). Analytical methods for microplastics in the environment: a review. *Environmental Chemistry Letters*, *21*(1), 383-401.

Jambeck, J. R., Geyer, R., Wilcox, C., Siegler, T. R., Perryman, M., Andrady, A., Narayan, R., & Law, K. L. (2015). Marine pollution. Plastic waste inputs from land into the ocean. *Science*, *347*(6223), 768-771.

Jandang, S., Alfonso, M. B., Nakano, H., Phinchan, N., Darumas, U., Viyakarn, V., Chavanich, S., & Isobe, A. (2024). Possible sink of missing ocean plastic: Accumulation patterns in reef-building corals in the Gulf of Thailand. *Science of the Total Environment*, *954*, 176210.

Jiang, L., Sun, Y.-F., Zhang, Y.-Y., Zhou, G.-W., Li, X.-B., McCook, L. J., Lian, J.-S., Lei, X.-M., Liu, S., Cai, L., Qian, P.-Y., & Huang, H. (2017). Impact of diurnal temperature fluctuations on larval settlement and growth of the reef coral *Pocillopora damicornis*. *Biogeosciences*, *14*(24), 5741-5752.

Jorissen, H., Galand, P. E., Bonnard, I., Meiling, S., Raviglione, D., Meistertzheim, A. L., Hedouin, L., Banaigs, B., Payri, C. E., & Nugues, M. M. (2021). Coral larval settlement preferences linked to crustose coralline algae with distinct chemical and microbial signatures. *Scientific Reports*, *11*(1), 14610.

Kaposi, K. L., Mos, B., Kelaher, B. P., & Dworjanyn, S. A. (2014). Ingestion of microplastic has limited impact on a marine larva. *Environmental Science & Technology*, *48*(3), 1638-1645.

Kruschke, J. K. (2010). What to believe: Bayesian methods for data analysis. *Trends in cognitive sciences*, *14*(7), 293-300.

Kruschke, J. K. (2015). *Doing Bayesian data analysis a tutorial with R, JAGS, and Stan* (2nd ed.). Academic Press.

Kruschke, J. K., Aguinis, H., & Joo, H. (2012). The Time Has Come: Bayesian Methods for Data Analysis in the Organizational Sciences. *Organizational Research Methods*, *15*(4), 722-752.

Kruschke, J. K., & Liddell, T. M. (2018). The Bayesian New Statistics: Hypothesis testing, estimation, meta-analysis, and power analysis from a Bayesian perspective. *Psychonomic bulletin & review*, *25*(1), 178-206.

Lanctot, C. M., Bednarz, V. N., Melvin, S., Jacob, H., Oberhaensli, F., Swarzenski, P. W., Ferrier-Pages, C., Carroll, A. R., & Metian, M. (2020). Physiological stress response of the scleractinian coral Stylophora pistillata exposed to polyethylene microplastics. *Environmental Pollution*, *263*(Pt A), 114559.

Lavers, J. L., & Bond, A. L. (2017). Exceptional and rapid accumulation of anthropogenic debris on one of the world's most remote and pristine islands. *Proceedings of the National Academy of Sciences*, *114*(23), 6052-6055.

Leung, M. M., Ho, Y. W., Lee, C. H., Wang, Y., Hu, M., Kwok, K. W. H., Chua, S. L., & Fang, J. K. (2021). Improved Raman spectroscopy-based approach to assess microplastics in seafood. *Environmental Pollution*, *289*, 117648.

Liang, J., Niu, T., Zhang, L., Yang, Y., Li, Z., Liang, Z., Yu, K., & Gong, S. (2025). Polystyrene microplastics exhibit toxic effects on the widespread coral symbiotic *Cladocopium goreaui*. *Environmental Research*, *268*, 120750.

Liang, T., Lei, Z., Fuad, M. T. I., Wang, Q., Sun, S., Fang, J. K., & Liu, X. (2022). Distribution and potential sources of microplastics in sediments in remote lakes of Tibet, China. *Science of the Total Environment*, *806*(Pt 2), 150526.

Lin, C., Kang, C.-M., Huang, C.-Y., Li, H.-H., & Tsai, S. (2022). Study on the Development and Growth of Coral Larvae. *Applied Sciences*, *12*(10), 5255.

Liu, C.-Y., Zhang, F., Sun, Y.-F., Yu, X.-L., & Huang, H. (2020). Effects of Nitrate Enrichment on Respiration, Photosynthesis, and Fatty Acid Composition of Reef Coral *Pocillopora damicornis* Larvae. *Frontiers in Marine Science*, *7*.

Liu, S. Y., Leung, M. M.-L., Fang, J. K.-H., & Chua, S. L. (2021). Engineering a microbial "trap and release" mechanism for microplastics removal. *Chemical Engineering Journal*, *404*, 127079.

Lo, H. S., Xu, X., Wong, C. Y., & Cheung, S. G. (2018). Comparisons of microplastic pollution between mudflats and sandy beaches in Hong Kong. *Environmental Pollution*, *236*, 208-217.

Mak, C. W., Tsang, Y. Y., Leung, M. M., Fang, J. K., & Chan, K. M. (2020). Microplastics from effluents of sewage treatment works and stormwater discharging into the Victoria Harbor, Hong Kong. *Marine Pollution Bulletin*, *157*, 111181.

Makowski, D., Ben-Shachar, M., & Lüdecke, D. (2019). bayestestR: Describing Effects and their Uncertainty, Existence and Significance within the Bayesian Framework. *Journal of open source software*, *4*(40), 1541.

Malik, M. H., Chan, S. A., Babalola, L. O., & Kaminski, M. A. (2022). Optimization of the acetic acid method for microfossil extraction from lithified carbonate rocks: Examples from the Jurassic and Miocene limestones of Saudi Arabia. *MethodsX*, *9*, 101828.

McCormick, M. I., Chivers, D. P., Ferrari, M. C. O., Blandford, M. I., Nanninga, G. B., Richardson, C., Fakan, E. P., Vamvounis, G., Gulizia, A. M., & Allan, B. J. M. (2020). Microplastic exposure interacts with habitat degradation to affect behaviour and survival of juvenile fish in the field. *Proceedings of the Royal Society B: Biological Sciences*, *287*(1937), 20201947.

McElreath, R. (2016). *Statistical rethinking : A Bayesian Course with Examples in R and Stan*. CRC Press/Taylor & Francis Group.

McKenna, S. A., Richmond, R. H., Roos, G., & Thomas, J. D. (2001). Assessing the effects of sewage on coral reefs: Developing techniques to detect stress before coral mortality. *Bulletin of Marine Science*, *69*(2), 517-523.

Mercado-Molina, A. E., Sabat, A. M., & Hernandez-Delgado, E. A. (2020). Population dynamics of diseased corals: Effects of a Shut Down Reaction outbreak in Puerto Rican *Acropora cervicornis*. *Advances in Marine Biology*, *87*(1), 61-82.

Morton, B. (1994). Hong Kong's coral communities: Status, threats and management plans. *Marine Pollution Bulletin*, *29*(1), 74-83.

Nakagawa, S., Schielzeth, H., & O'Hara, R. B. (2013). A general and simple method for obtaining R2 from generalized linear mixed-effects models. *Methods in Ecology and Evolution*, *4*(2), 133-142.

Naumann, M. S., Niggl, W., Laforsch, C., Glaser, C., & Wild, C. (2009). Coral surface area quantification–evaluation of established techniques by comparison with computer tomography. *Coral Reefs*, *28*, 109-117.

Negri, A. P., & Hoogenboom, M. O. (2011). Water contamination reduces the tolerance of coral larvae to thermal stress. *PLoS One*, *6*(5), e19703.

Ng, M. S., & Todd, P. A. (2023). The comparative effects of chronic microplastic and sediment deposition on the scleractinian coral Merulina ampliata. *Marine Environmental Research*, *191*, 106135.

Ng, T. Y., & Ang, P. (2016). Low symbiont diversity as a potential adaptive strategy in a marginal non-reefal environment: a case study of corals in Hong Kong. *Coral Reefs*, *35*(3), 941-957.

Okubo, N., Takahashi, S., & Nakano, Y. (2018). Microplastics disturb the anthozoan-algae symbiotic relationship. *Marine Pollution Bulletin*, *135*, 83-89.

Pantos, O. (2022). Microplastics: impacts on corals and other reef organisms. *Emerging Topics in Life Sciences*, *6*(1), 81-93.

Perez, K., 3rd, Rodgers, K. S., Jokiel, P. L., Lager, C. V., & Lager, D. J. (2014). Effects of terrigenous sediment on settlement and survival of the reef coral *Pocillopora damicornis*. *PeerJ*, *2*, e387.

Petersen, D., Laterveer, M., & Schuhmacher, H. (2004). Innovative substrate tiles to spatially control larval settlement in coral culture. *Marine Biology*, *146*, 937-942.

Plastics Europe. (2021). In *Plastics – The Facts 2021. An Analysis of European Plastics Production, Demand and Waste Data* (pp. 33). Brussels: Plastics Europe.

Raguso, C., Saliu, F., Lasagni, M., Galli, P., Clemenza, M., & Montano, S. (2022). First detection of microplastics in reef-building corals from a Maldivian atoll. *Marine Pollution Bulletin*, *180*, 113773.

Rani, M., Ducoli, S., Depero, L. E., Prica, M., Tubic, A., Ademovic, Z., Morrison, L., & Federici, S. (2023). A Complete Guide to Extraction Methods of Microplastics from Complex Environmental Matrices. *Molecules*, *28*(15).

Reichert, J., Arnold, A. L., Hammer, N., Miller, I. B., Rades, M., Schubert, P., Ziegler, M., & Wilke, T. (2022). Reef-building corals act as long-term sink for microplastic. *Global Change Biology*, *28*(1), 33-45.

Reichert, J., Arnold, A. L., Hoogenboom, M. O., Schubert, P., & Wilke, T. (2019). Impacts of microplastics on growth and health of hermatypic corals are species-specific. *Environmental Pollution*, *254*(Pt B), 113074.

Reichert, J., Schellenberg, J., Schubert, P., & Wilke, T. (2016). 3D scanning as a highly precise, reproducible, and minimally invasive method for surface area and volume measurements of scleractinian corals. *Limnology and oceanography, Methods*, *14*(8), 518-526.

Reichert, J., Schellenberg, J., Schubert, P., & Wilke, T. (2018). Responses of reef building corals to microplastic exposure. *Environmental Pollution*, *237*, 955-960.

Rocha, R. J. M., Rodrigues, A. C. M., Campos, D., Cicero, L. H., Costa, A. P. L., Silva, D. A. M., Oliveira, M., Soares, A., & Patricio Silva, A. L. (2020). Do microplastics affect the zoanthid *Zoanthus sociatus*? *Science of the Total Environment*, *713*, 136659.

Ross, P. S., Chastain, S., Vassilenko, E., Etemadifar, A., Zimmermann, S., Quesnel, S. A., Eert, J., Solomon, E., Patankar, S., Posacka, A. M., & Williams, B. (2021). Pervasive distribution of polyester fibres in the Arctic Ocean is driven by Atlantic inputs. *Nature Communications*, *12*(1), 106.

Rotjan, R. D., Sharp, K. H., Gauthier, A. E., Yelton, R., Lopez, E. M. B., Carilli, J., Kagan, J. C., & Urban-Rich, J. (2019). Patterns, dynamics and consequences of microplastic ingestion by the temperate coral, *Astrangia poculata*. *Proceedings of the Royal Society B: Biological Sciences*, *286*(1905), 20190726.

Savinelli, B., Vega Fernandez, T., Galasso, N. M., D'Anna, G., Pipitone, C., Prada, F., Zenone, A., Badalamenti, F., & Musco, L. (2020). Microplastics impair the feeding performance of a Mediterranean habitat-forming coral. *Marine Environmental Research*, *155*, 104887.

Schielzeth, H. (2010). Simple means to improve the interpretability of regression coefficients. *Methods in Ecology and Evolution*, *1*(2), 103-113.

Schneider, C. A., Rasband, W. S., & Eliceiri, K. W. (2012). NIH Image to ImageJ: 25 years of image analysis. *Nature Methods*, *9*(7), 671-675.

Schwarz, J. A., Krupp, D. A., & Weis, V. M. (1999). Late Larval Development and Onset of Symbiosis in the Scleractinian Coral *Fungia scutaria*. *Biology Bulletin*, *196*(1), 70-79.

Sebens, K. P., Grace, S. P., Helmuth, B., Maney, E. J., & Miles, J. S. (1998). Water flow and prey capture by three scleractinian corals, *Madracis mirabilis*, *Montastrea cavernosa* and *Porites porites*, in a field enclosure. *Marine Biology*, *131*(2), 347-360.

Soares, M. O., Matos, E., Lucas, C., Rizzo, L., Allcock, L., & Rossi, S. (2020). Microplastics in corals: An emergent threat. *Marine Pollution Bulletin*, *161*(Pt A), 111810.

Su, Y., Zhang, K., Zhou, Z., Wang, J., Yang, X., Tang, J., Li, H., & Lin, S. (2020). Microplastic exposure represses the growth of endosymbiotic dinoflagellate *Cladocopium goreaui* in culture through affecting its apoptosis and metabolism. *Chemosphere*, *244*, 125485.

Syakti, A. D., Jaya, J. V., Rahman, A., Hidayati, N. V., Raza'i, T. S., Idris, F., Trenggono, M., Doumenq, P., & Chou, L. M. (2019). Bleaching and necrosis of staghorn coral (*Acropora formosa*) in laboratory assays: Immediate impact of LDPE microplastics. *Chemosphere*, *228*, 528-535.

Tang, C. H., Lin, C. Y., Li, H. H., & Kuo, F. W. (2024). Microplastics elicit an immune-agitative state in coral. *Science of the Total Environment*, *908*, 168406.

Tang, J., Wu, Z., Wan, L., Cai, W., Chen, S., Wang, X., Luo, J., Zhou, Z., Zhao, J., & Lin, S. (2021). Differential enrichment and physiological impacts of ingested microplastics in scleractinian corals in situ. *J Hazard Mater*, *404*(Pt B), 124205.

Tebben, J., Motti, C. A., Siboni, N., Tapiolas, D. M., Negri, A. P., Schupp, P. J., Kitamura, M., Hatta, M., Steinberg, P. D., & Harder, T. (2015). Chemical mediation of coral larval settlement by crustose coralline algae. *Scientific Reports*, *5*, 10803.

Terrell, A. P., Marangon, E., Webster, N. S., Cooke, I., & Quigley, K. M. (2023). The promotion of stress tolerant Symbiodiniaceae dominance in juveniles of two coral species under simulated future conditions of ocean warming and acidification. *Frontiers in Ecology and Evolution*, *11*.

Tietjen, K. L., Perks, N. F., O'Brien, N. C., & Baum, J. K. (2025). Impacts of a prolonged marine heatwave and chronic local human disturbance on juvenile coral assemblages. *PLoS One*, *20*(2), e0300084.

Travaglione, N., Evans, R., Moustaka, M., Cuttler, M., Thomson, D. P., Tweedley, J., & Wilson, S. (2023). Scleractinian corals rely on heterotrophy in highly turbid environments. *Coral Reefs*, *42*(5), 997-1010.

Tsang, R. H. L., & Ang, P., Jr. (2019). Resistance to temperature stress and Drupella corallivory may promote the dominance of *Platygyra acuta* in the marginal coral communities in Hong Kong. *Marine Environmental Research*, *144*, 20-27.

Tsang, Y. Y., Mak, C. W., Liebich, C., Lam, S. W., Sze, E. T., & Chan, K. M. (2017). Microplastic pollution in the marine waters and sediments of Hong Kong. *Marine Pollution Bulletin*, *115*(1-2), 20-28.

van de Schoot, R., Depaoli, S., King, R., Kramer, B., Märtens, K., Tadesse, M. G., Vannucci, M., Gelman, A., Veen, D., Willemsen, J., & Yau, C. (2021). Bayesian statistics and modelling. *Nature Reviews Methods Primers*, *1*(1), 1.

Veal, C. J., Carmi, M., Fine, M., & Hoegh-Guldberg, O. (2010). Increasing the accuracy of surface area estimation using single wax dipping of coral fragments. *Coral Reefs*, *29*(4), 893-897.

Vermeij, M. J. A., Frade, P. R., & Bak, R. P. M. (2013). Zooxanthellae presence acts as a settlement cue for aposymbiotic planulae of the Caribbean Coral *Montastraea faveolata*. *Caribbean Journal of Science*, *47*(1), 31-36.

Webster, F. J., Babcock, R. C., Van Keulen, M., & Loneragan, N. R. (2015). Macroalgae inhibits larval settlement and increases recruit mortality at Ningaloo Reef, Western Australia. *PLoS One*, *10*(4), e0124162.

Webster, N. S., Smith, L. D., Heyward, A. J., Watts, J. E., Webb, R. I., Blackall, L. L., & Negri, A. P. (2004). Metamorphosis of a scleractinian coral in response to microbial biofilms. *Applied and Environmental Microbiology*, *70*(2), 1213-1221.

Winkler, N. S., Pandolfi, J. M., & Sampayo, E. M. (2015). *Symbiodinium* identity alters the temperature-dependent settlement behaviour of *Acropora millepora* coral larvae before the onset of symbiosis. *Proc Biol Sci*, *282*(1801), 20142260.

Yeung, Y. H., Xie, J. Y., Kwok, C. K., Kei, K., Ang, P., Jr., Chan, L. L., Dellisanti, W., Cheang, C. C., Chow, W. K., & Qiu, J. W. (2021). Hong Kong's subtropical scleractinian coral communities: Baseline, environmental drivers and management implications. *Marine Pollution Bulletin*, *167*, 112289.

Yuyama, I., Ishikawa, M., Nozawa, M., Yoshida, M. A., & Ikeo, K. (2018). Transcriptomic changes with increasing algal symbiont reveal the detailed process underlying establishment of coral-algal symbiosis. *Scientific Reports*, *8*(1), 16802.

Zhang, K., Hamidian, A. H., Tubic, A., Zhang, Y., Fang, J. K. H., Wu, C., & Lam, P. K. S. (2021). Understanding plastic degradation and microplastic formation in the environment: A review. *Environmental Pollution*, *274*, 116554.

Zhou, Z., Tang, J., Cao, X., Wu, C., Cai, W., & Lin, S. (2023). High Heterotrophic Plasticity of Massive Coral *Porites pukoensis* Contributes to Its Tolerance to Bioaccumulated Microplastics. *Environmental Science & Technology*, *57*(8), 3391-3401.

Zweifler, A., Browne, N. K., Levy, O., Hovey, R., & O'Leary, M. (2024). *Acropora tenuis* energy acquisition along a natural turbidity gradient. *Frontiers in Marine Science*, *11*.